Toward a finer understanding the nucleon with Volker in charge

Strong QCD from Nucleon Structure Experiments 2019
6-9 November 2019 Jefferson Lab

Keith Griffioen
College of William & Mary griff@physics.wm.edu

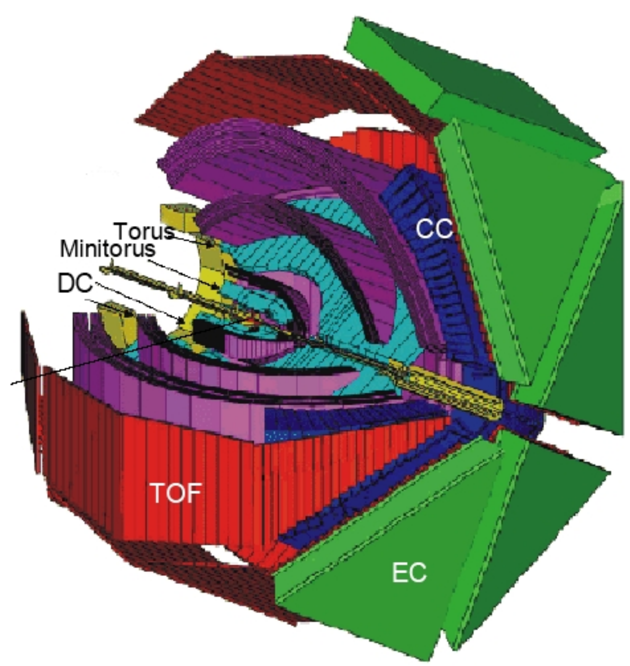

November 17, 2019

Volker D. Burkert

Volker Burkert joined Jefferson Lab in 1985 as staff scientist. He worked initially on the development of the CLAS detector system, where he focused on detectors needed for high luminosity electron beam operation. In 2003 he was appointed head of the Hall B department, where he is leading a team of 40 physicists, engineers and technicians in the implementation and operation of Hall B and its unique CLAS detector system. The research with CLAS focuses on the structure of nucleons and nuclei using electromagnetic beam and polarized targets. In the early 2000 Volker developed the concept of the CLAS12 detector, which is now under construction, and will serve a large program at 12 GeV aimed at spatial and momentum imaging of the nucleon, hadron spectroscopy, and QCD effects in nuclei. Before coming to JLab, Volker received a Ph.D. from Bonn University in 1975, where he subsequently worked as a postdoc and assistant professor studying nucleon excitations, and using polarized deuteron targets. He led the effort to measure the motion of polarized electrons in a synchrotron for use in electron scattering experiments. From 1979-1982 he worked at CERN on hard scattering processes that resulted in the first determination of the proton's gluon structure function. He is author of over 200 publications in refereed journals, contributed chapters in books, and was elected Fellow of the APS in 2004. He is serving as referee for physics journals and for research funding.

12000 Jefferson Avenue, Newport News, VA 23606
Phone: (757) 269-7621 Fax: (757) 269-7848

contact Volker Burkert
updated June 25, 2013

From 2003 to 2019 Volker has made CLAS physics possible
We are all deeply grateful!

Spectator Protons

Electron scattering from high-momentum neutrons in deuterium

A. V. Klimenko,[27,*] S. E. Kuhn,[27,†] C. Butuceanu,[38] K. S. Egiyan,[39] K. A. Griffioen,[38] G. Adams,[29] P. Ambrozewicz,[9] M. Anghinolfi,[15] G. Asryan,[39] H. Avakian,[34] H. Bagdasaryan,[27,39] N. Baillie,[38] J. P. Ball,[1] N. A. Baltzell,[33] S. Barrow,[10]

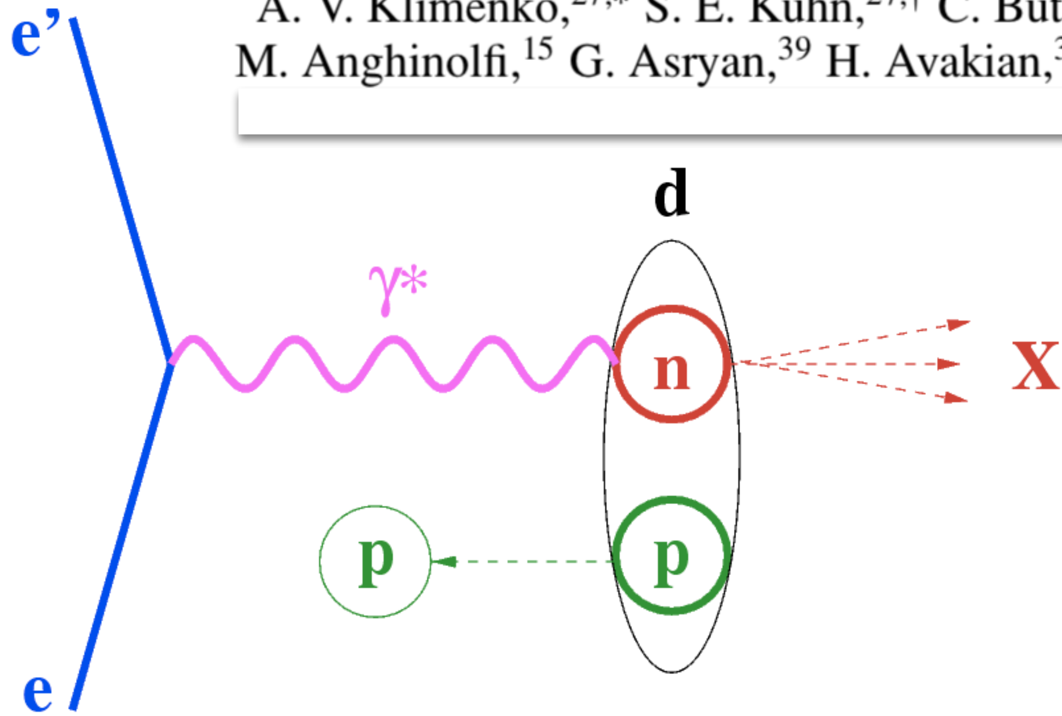

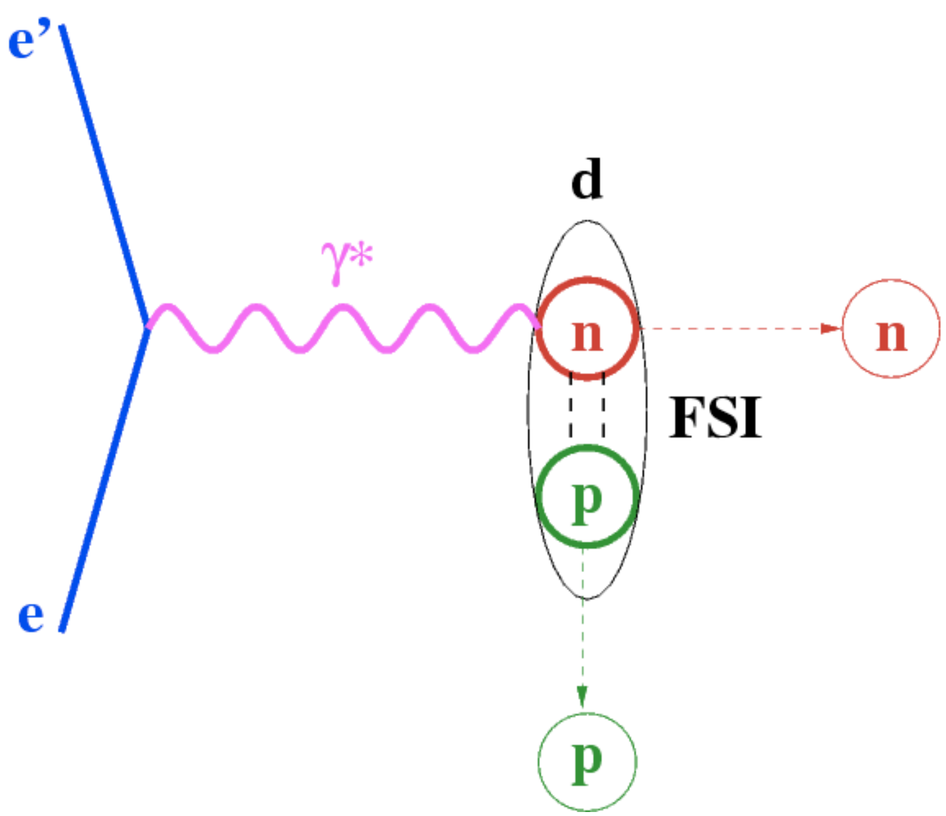

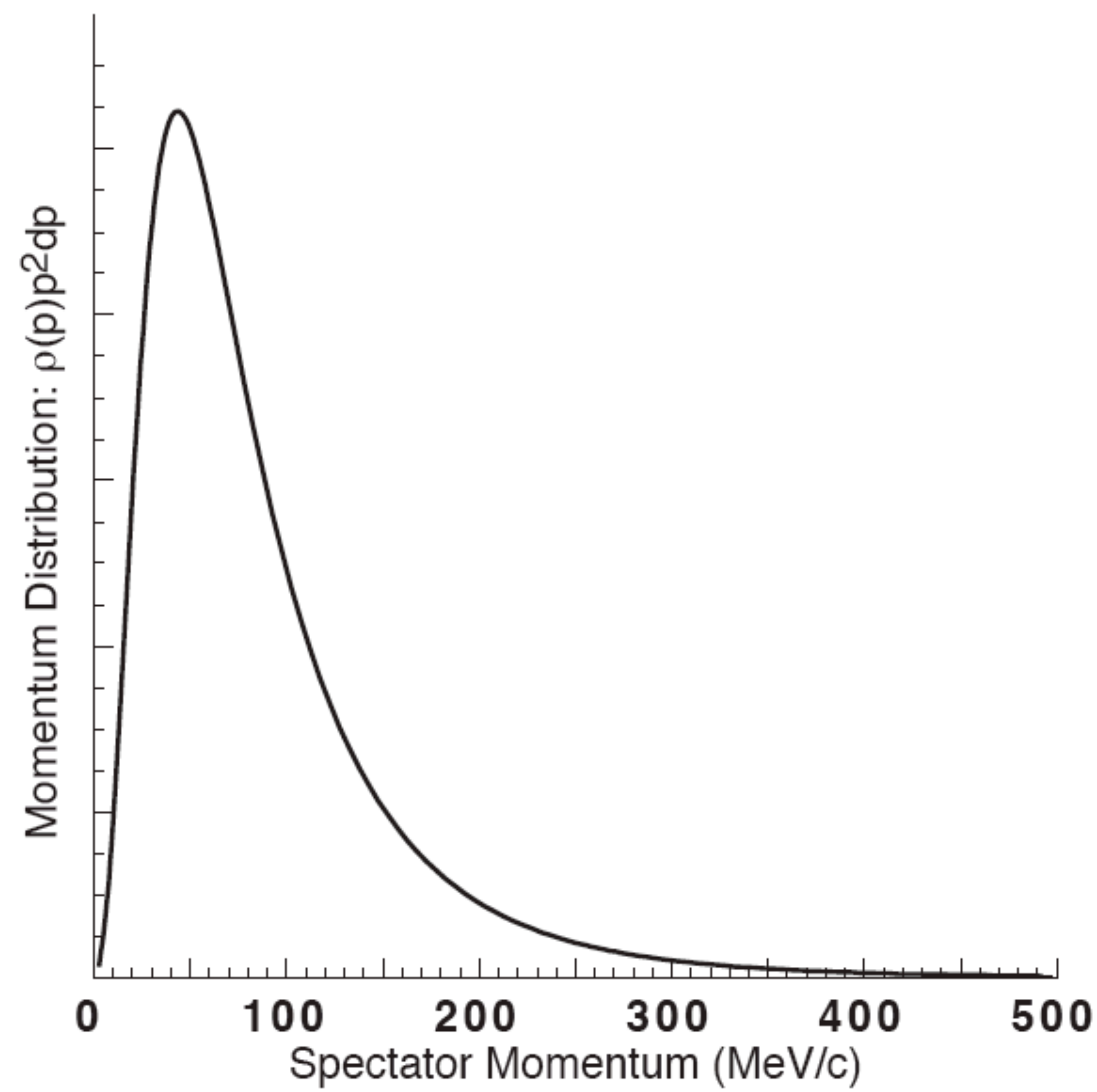

Final State Interactions

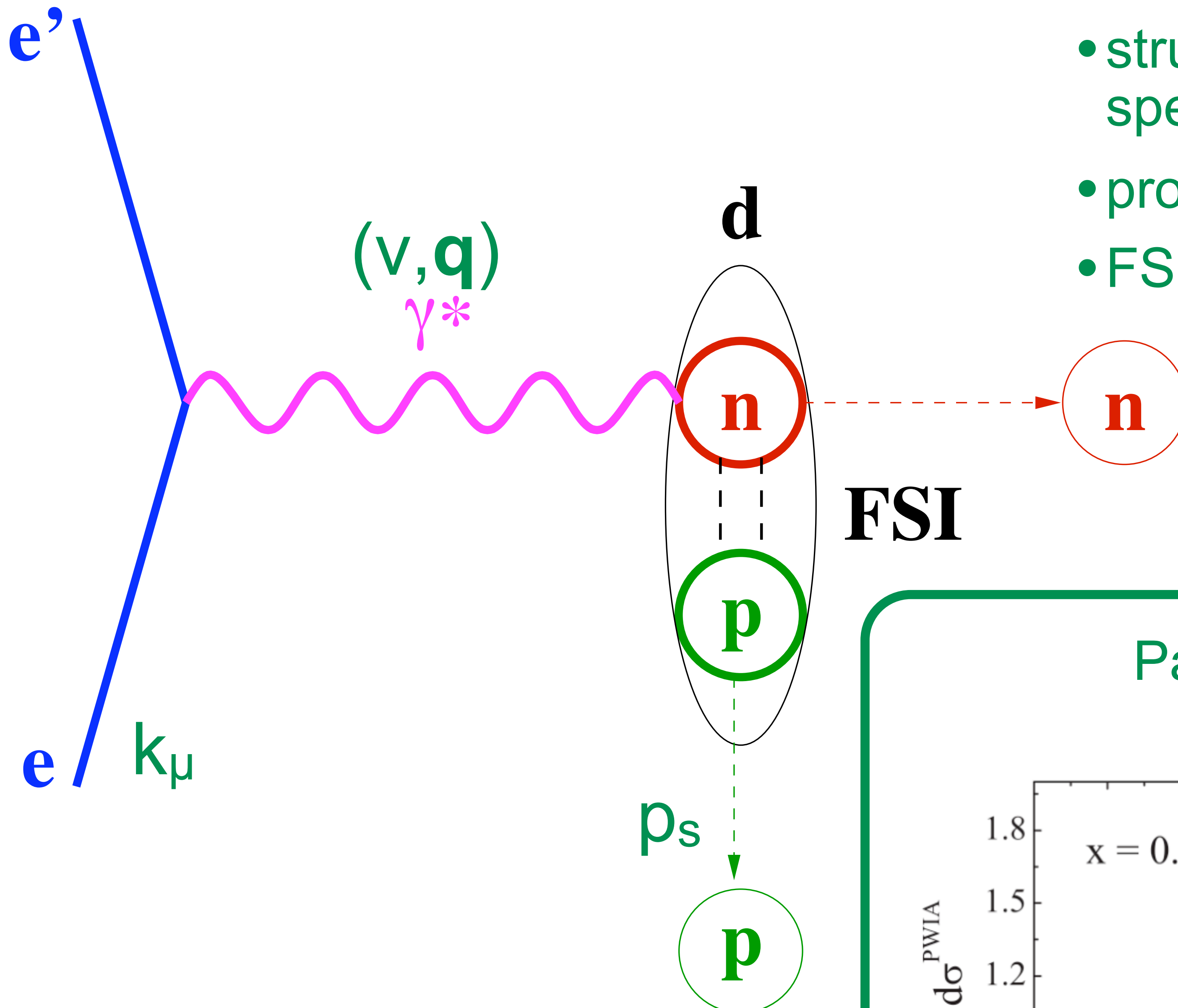

- struck neutron can interact with the spectator proton
- proton momentum is enhanced
- FSIs are small at low p_s and large Θ_{pq}

Palli et al, PRC80(09)054610

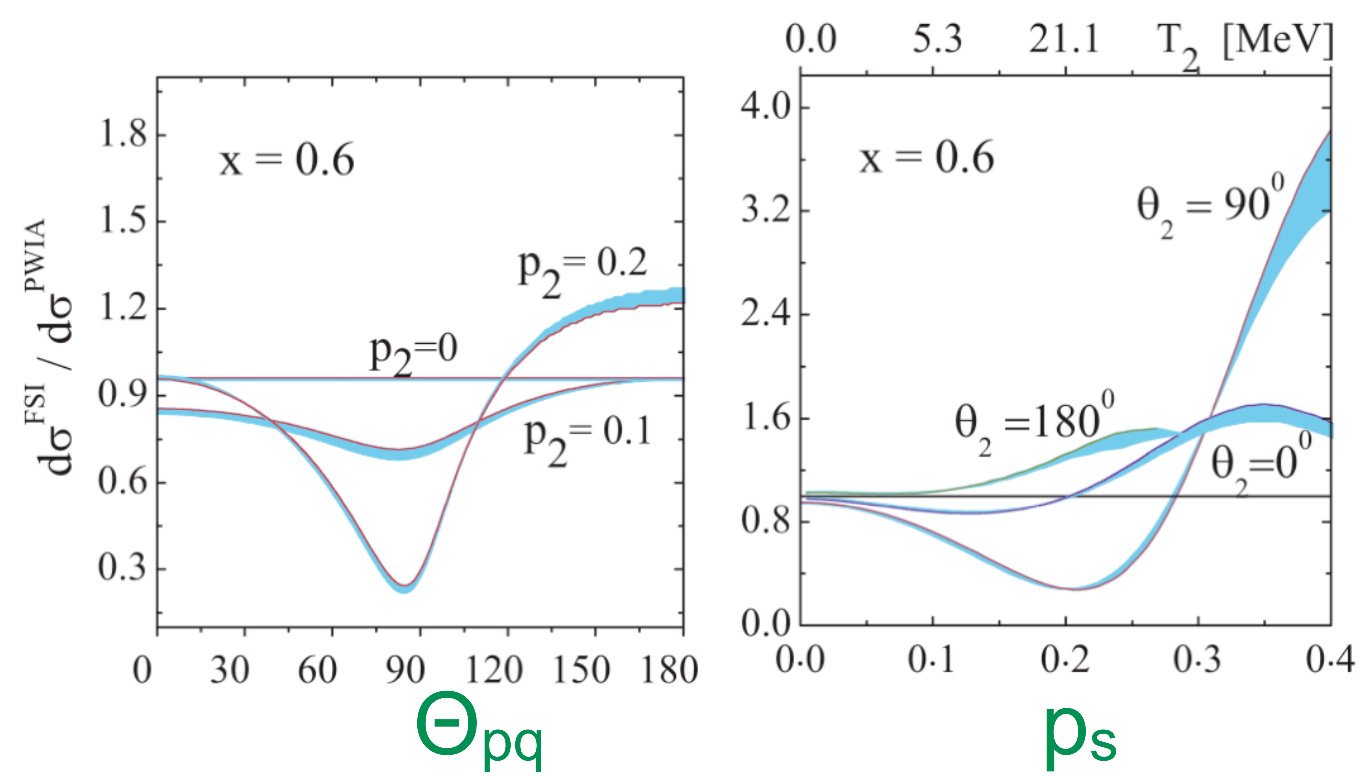

- several groups have calculated FSIs
- $\Theta_{pq} > 110^o$ minimizes FSIs

d(e,e'p$_s$)X

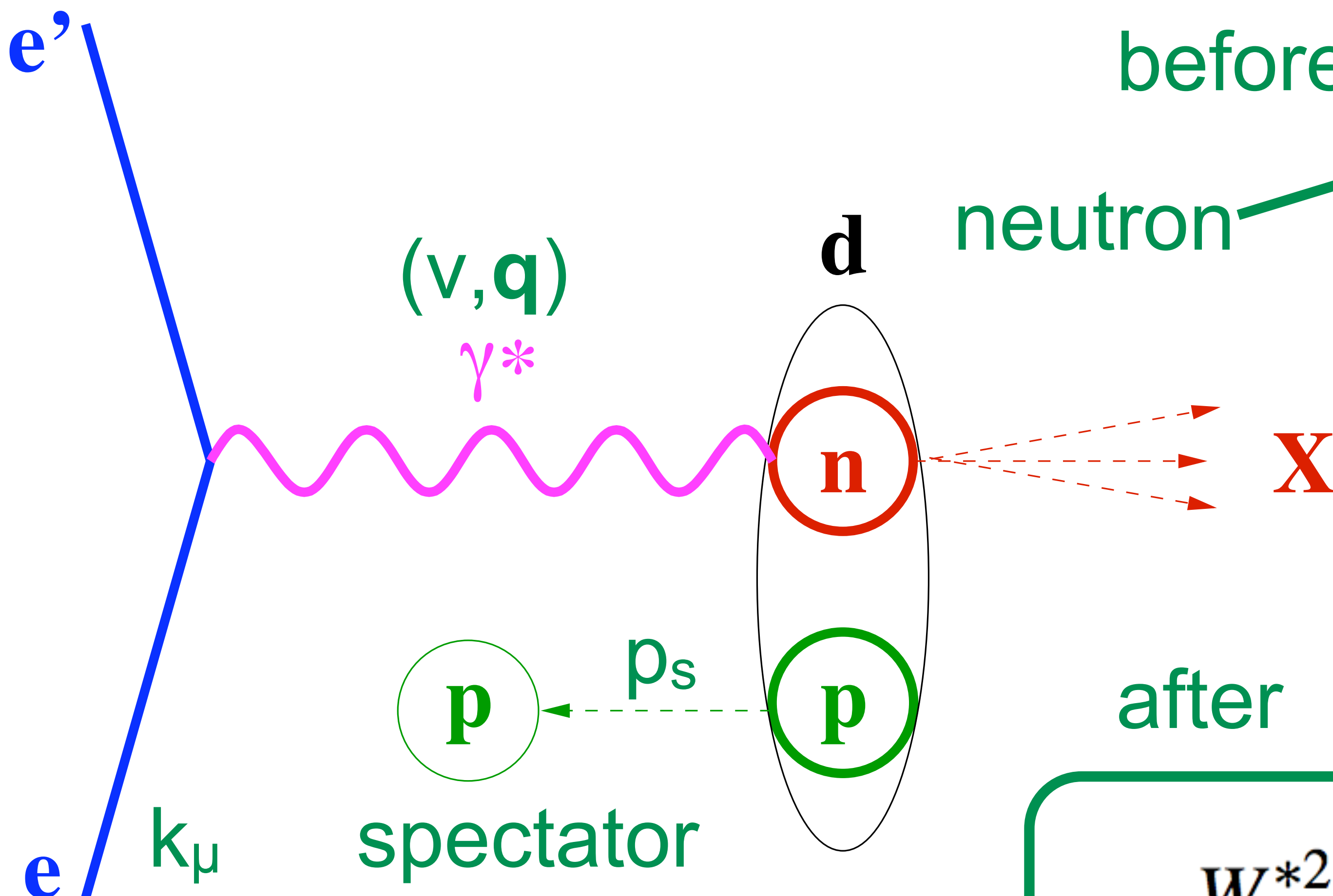

before

$$p_N^\mu = (M_d - E_s, -\vec{p}_s)$$

$$E_p + E_n = M_d$$

$$E^* = M_d - \sqrt{M_s^2 + p_s^2}$$

$$M^{*2} = (M_d - E_s)^2 - \vec{p}_s^{\,2}$$

after

$$W^{*2} \approx M^{*2} - Q^2 + 2M\nu\,(2 - \alpha_s)$$

$$\alpha_s = \frac{E_s - p_{s_{||}}}{M_s}$$

$$x^* = \frac{Q^2}{2p_N^\mu q^\mu} \approx \frac{Q^2}{2M\nu(2-\alpha_s)} = \frac{x}{2-\alpha_s}$$

- plane-wave impulse approximation
- backward-emitted p is spectator
- struck neutron is off-shell
- momenta are equal and opposite
- Lorentz invariants are corrected for initial neutron 4-momentum

Electron scattering from high-momentum neutrons in deuterium

A. V. Klimenko,[27,*] S. E. Kuhn,[27,†] C. Butuceanu,[38] K. S. Egiyan,[39] K. A. Griffioen,[38] G. Adams,[29] P. Ambrozewicz,[9]
M. Anghinolfi,[15] G. Asryan,[39] H. Avakian,[34] H. Bagdasaryan,[27,39] N. Baillie,[38] J. P. Ball,[1] N. A. Baltzell,[33] S. Barrow,[10]

Modification of Bound Neutrons in thD(e,e'p_s)

- Experiment 94-102 at Jefferson Lab
- Run period "E6" in Hall B (CLAS)
- 5.75 GeV / 7 nA Electrons on a 5 cm long LD_2 target => L=10^{34}/cm^2s
- 8 calendar weeks in spring of 2002; 4.5 billion triggers
- CLAS-Collaboration and 2 Ph.D. students:
  Dr. Alexei Klimenko and Dr. Cornel Butuceanu
- Detected backward proton

Results: Momentum Distribution

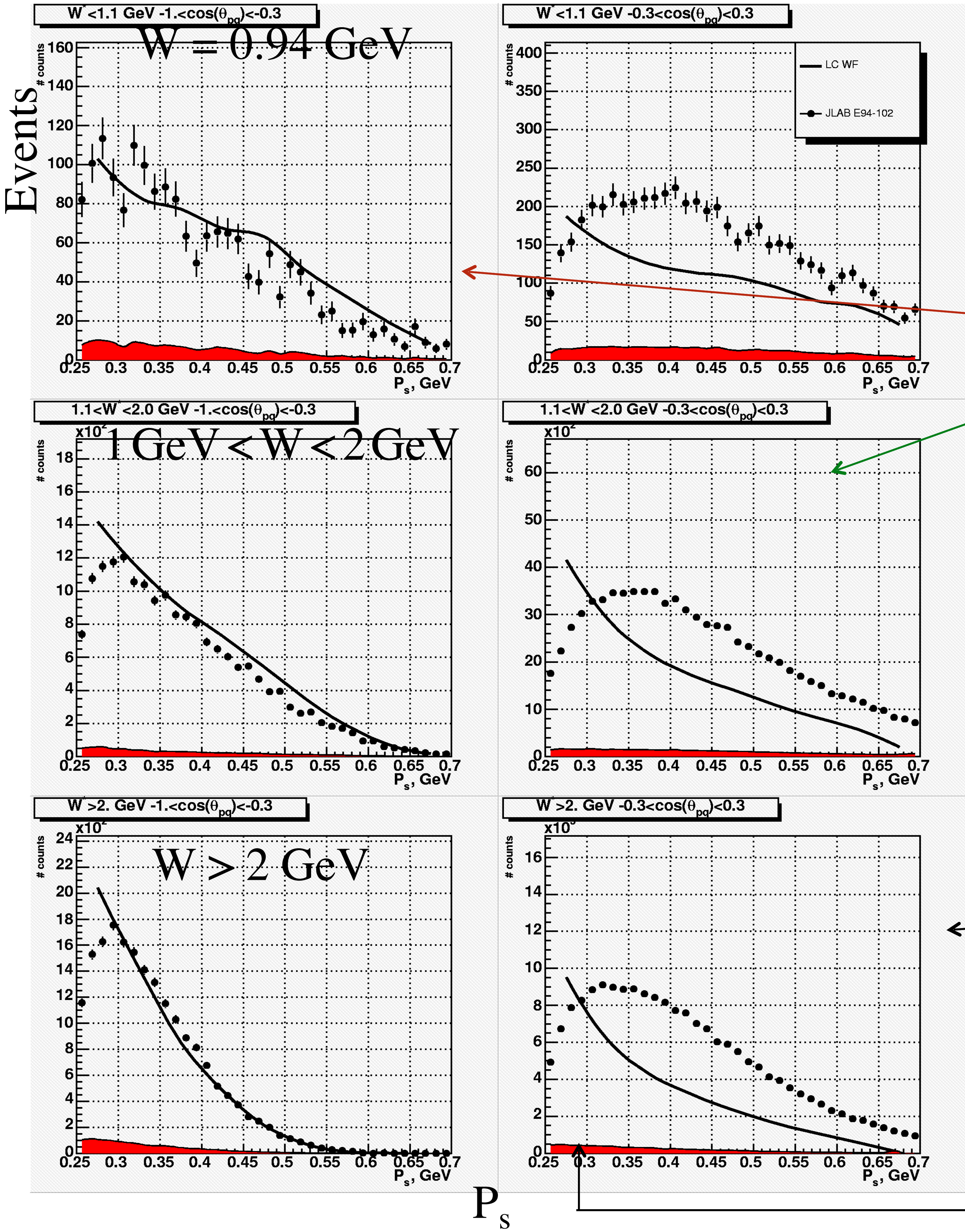

Vertical axis: Number of events

Horizontal axis: Proton momenta from 250 to 700 MeV/c

Left: Angular range > 107.5º
Right: Angular range 72.5º - 107.5º

3 different ranges in the final state mass W of the unobserved struck neutrons

PWIA model with “light cone”-wave function for deuterium

700 MeV/c

250 MeV/c

Publisher's Note: Measurement of the Neutron F_2 Structure Function via Spectator Tagging with CLAS [Phys. Rev. Lett. 108, 142001 (2012)]

N. Baillie, S. Tkachenko, J. Zhang, P. Bosted, S. Bültmann, M. E. Christy, H. Fenker, K. A. Griffioen, C. E. Keppel,

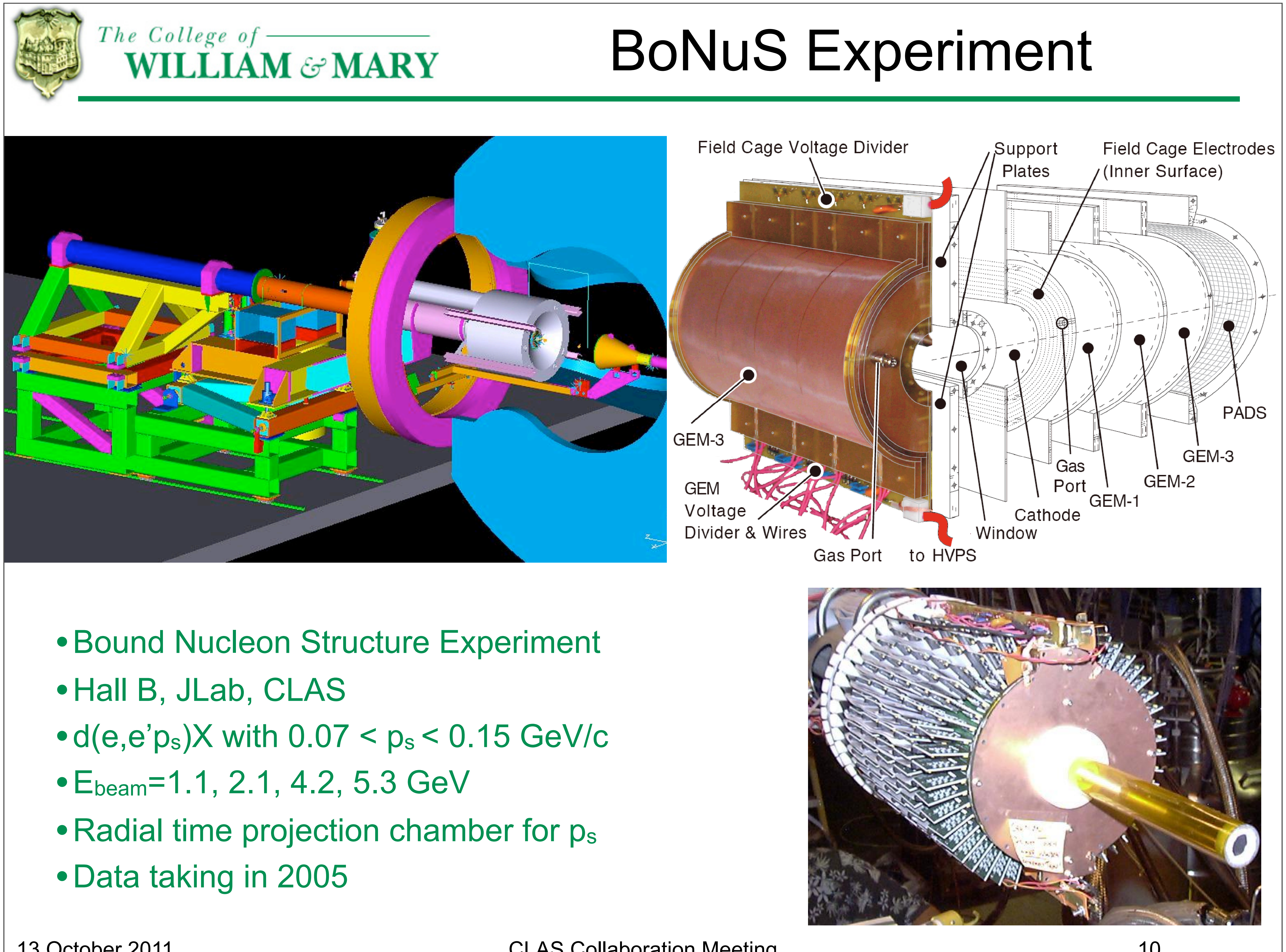

The College of WILLIAM & MARY

BoNuS RTPC Performance

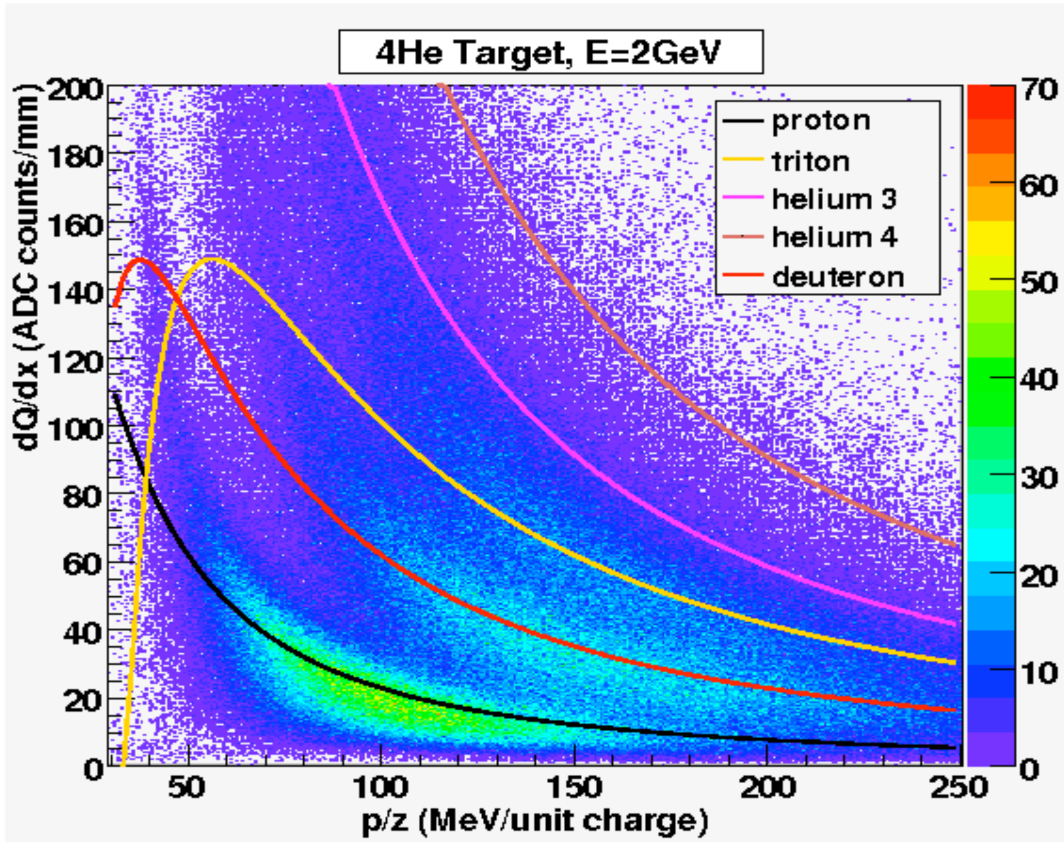

- upper left: dE/dx vs. p/Z for He target
- lower left: dE/dx vs. p for deuterium target
- below RTPC+CLAS resolution for common e^- events

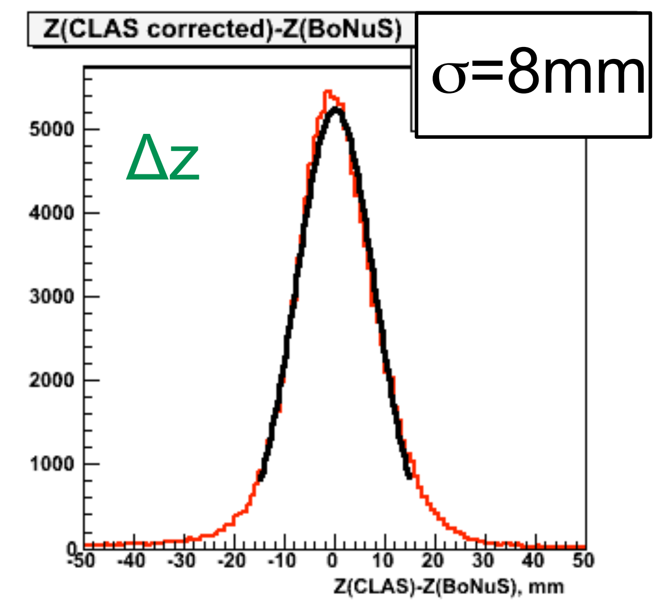

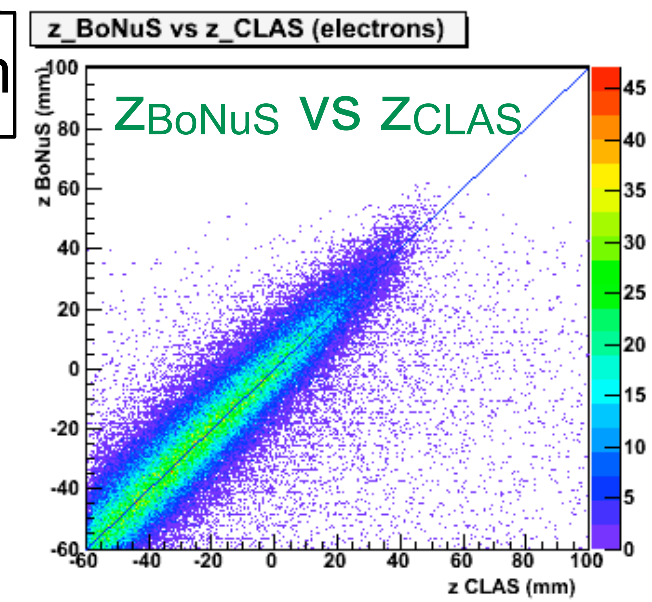

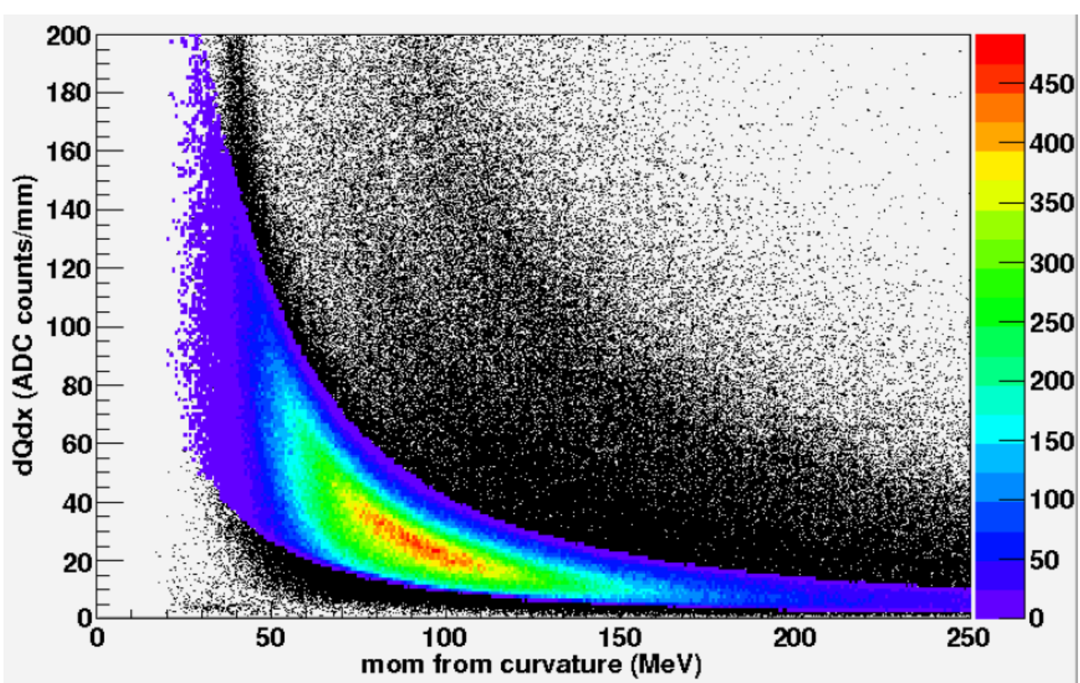

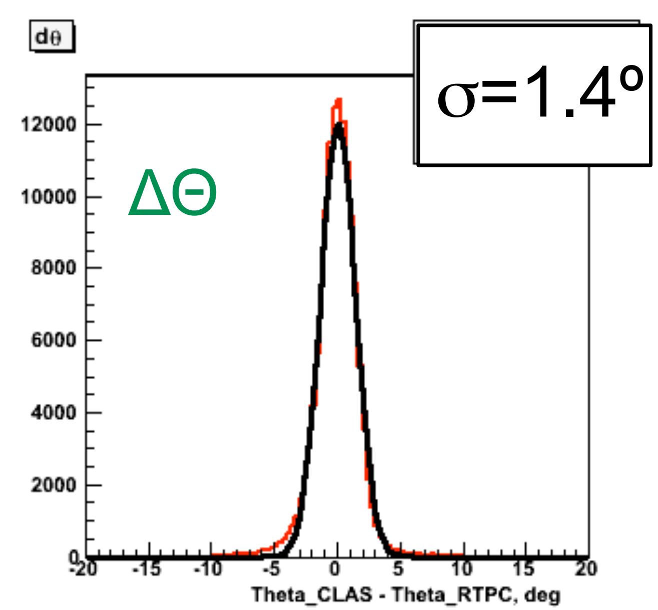

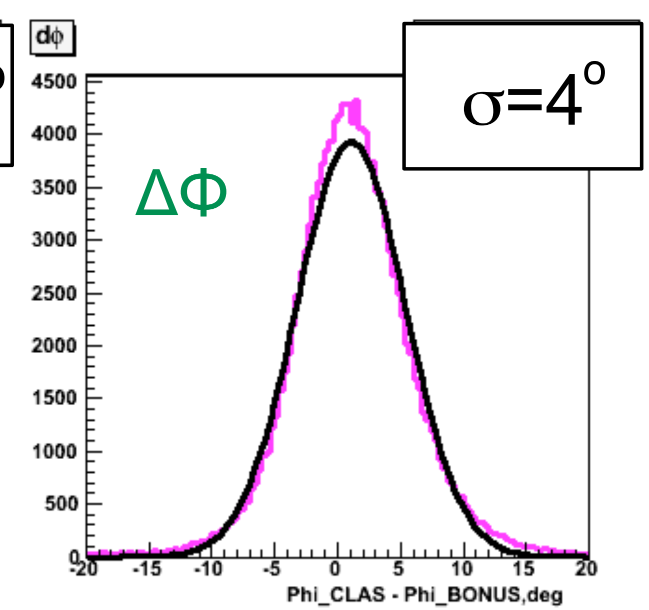

BoNuS Kinematic Correction

- Very Important Protons $70 < p_s < 100$ MeV/c
- Corrections make resonances stand out
- F_2^n/F_2^p can be measured at high x*

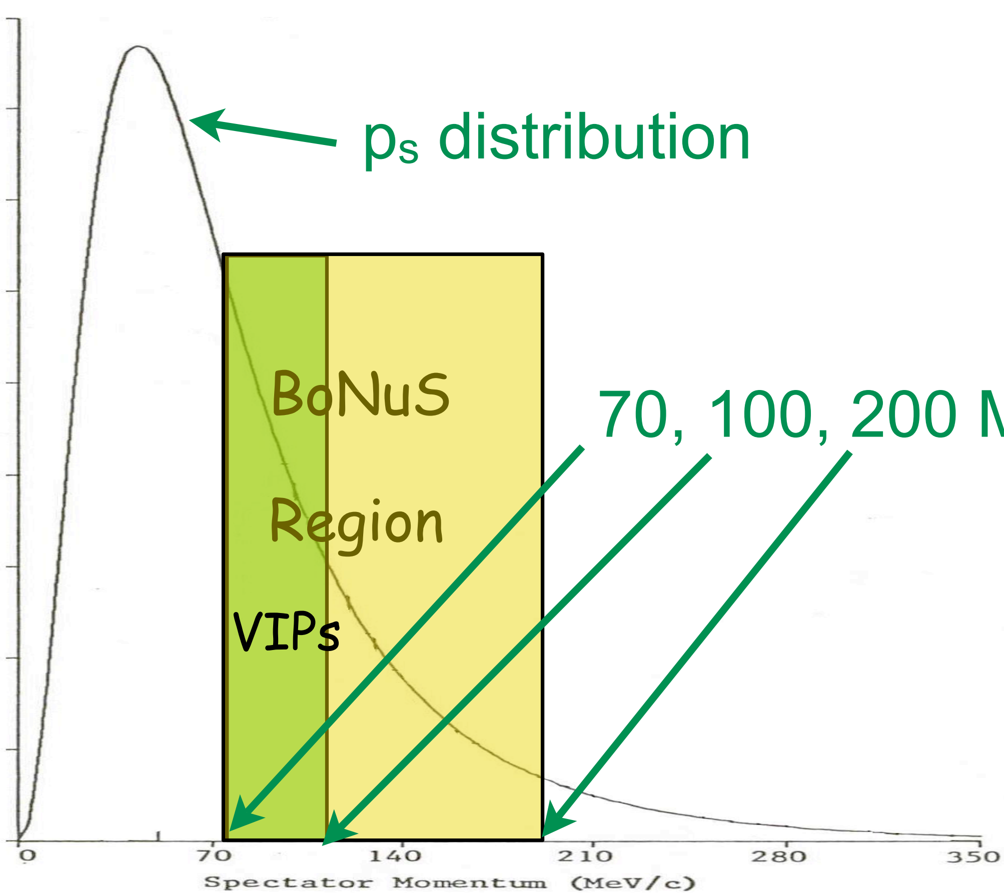

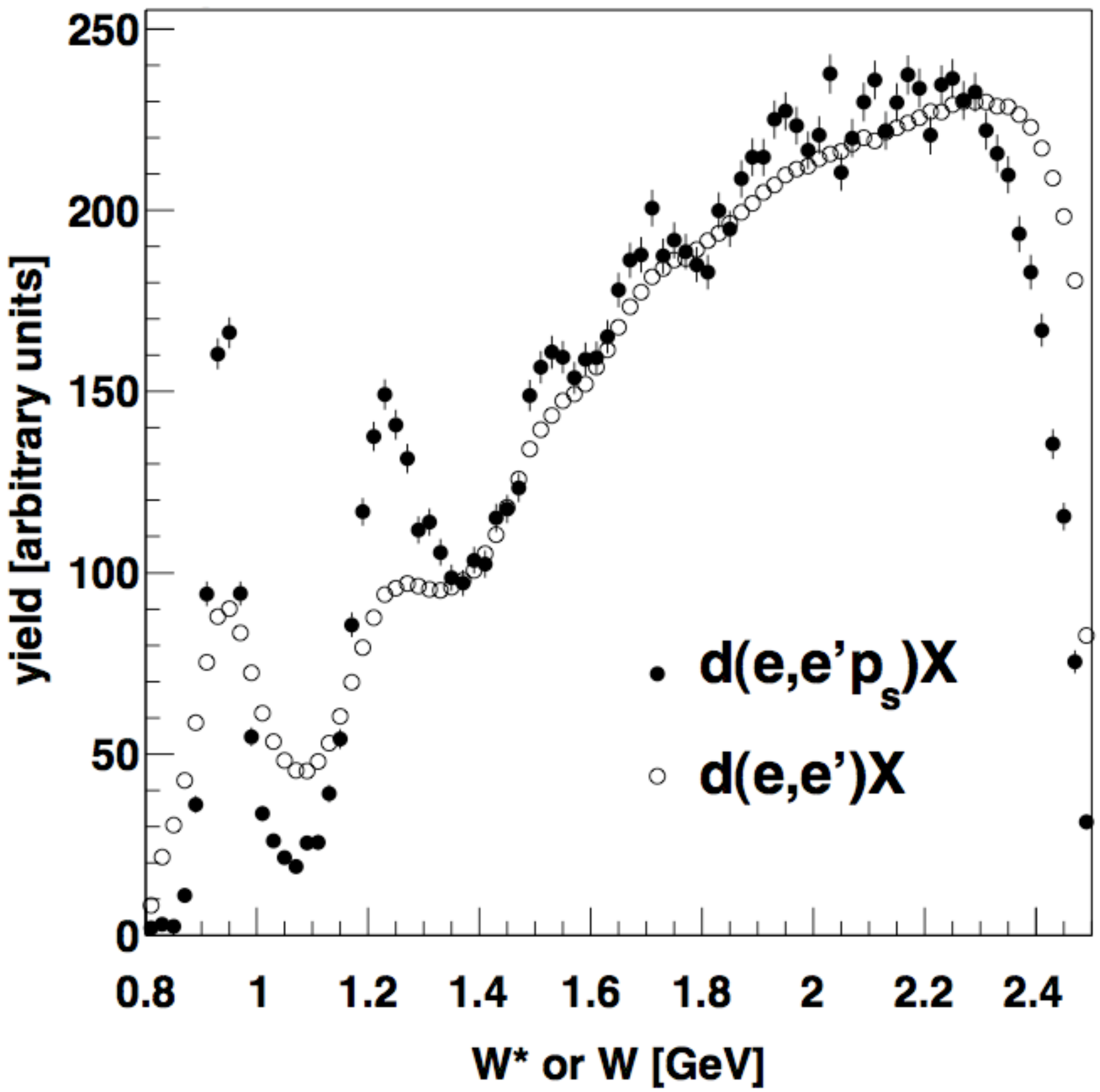

Accidental Backgrounds

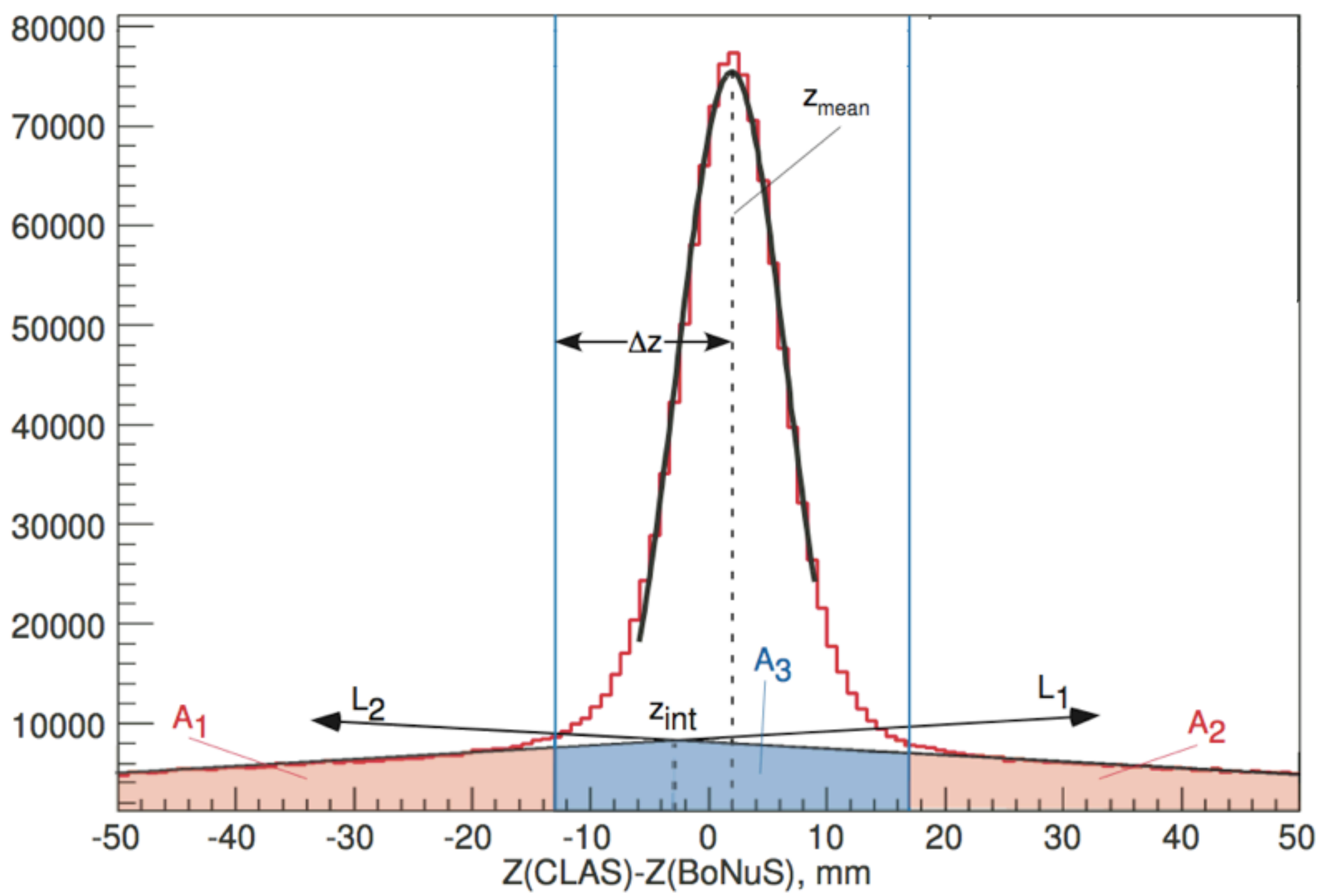

- Z is the position along the beam direction
- Tracking of the electron gives Z(CLAS)
- Tracking of the spectator proton gives Z(BoNuS)
- ΔZ=Z(CLAS)-Z(BoNuS) shows a coincidence peak and a triangular background
- Fits to the triangular background allows us to measure backgrounds underneath the peak
- Blue area = R_{bg} x Pink area
- R_{bg} is independent of kinematics

BoNuS F_2^n/F_2^p

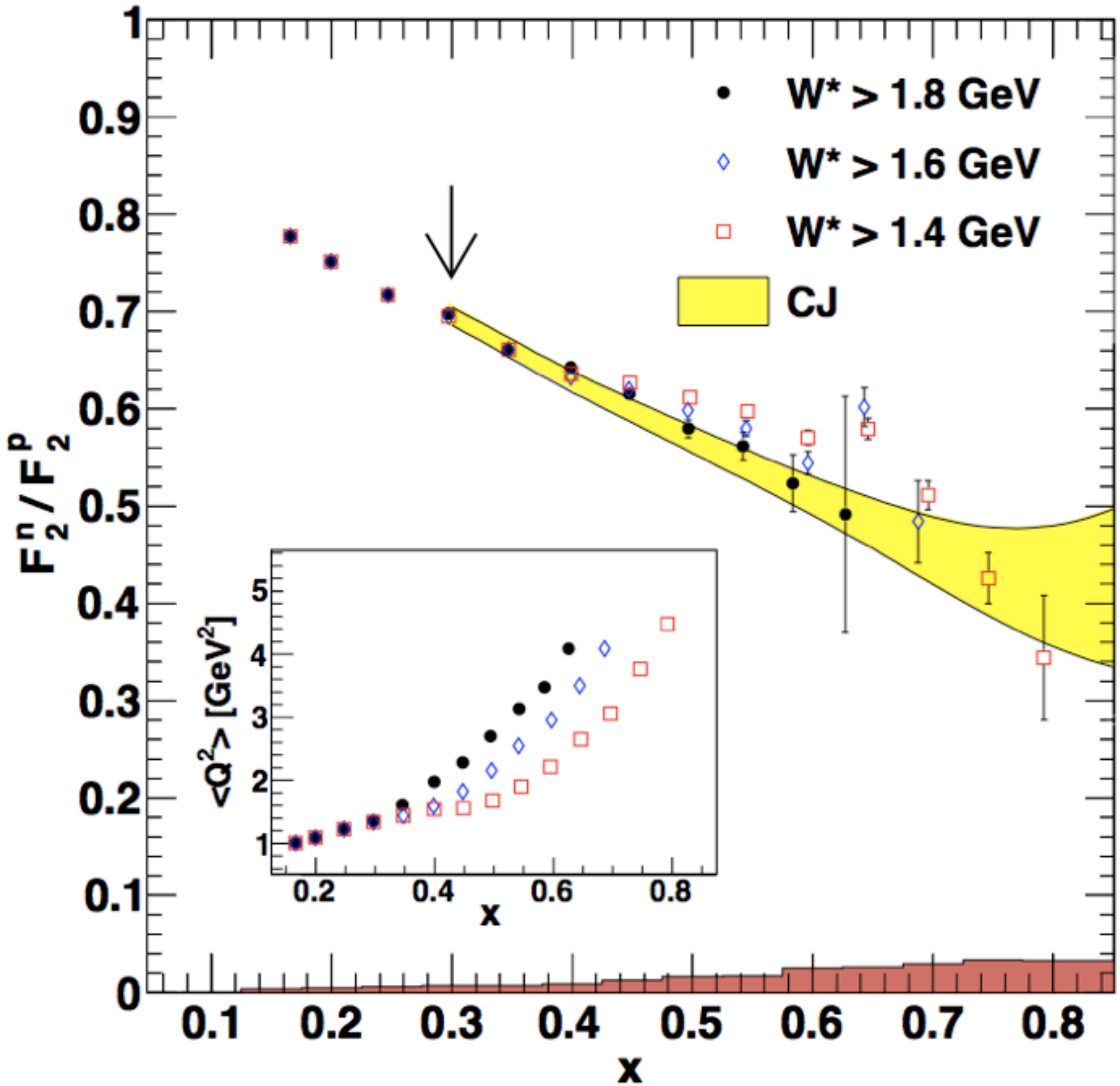

- F_2^n/F_2^n vs. x
- Curves are CETQ error bands
- CETQ cuts off at low x because Q^2 is too low
- Lower cuts in W* imply higher x but the inclusion of resonance contributions.
- Results are consistent with CETQ trends at high x.

The College of WILLIAM & MARY

BoNuS F_2^n

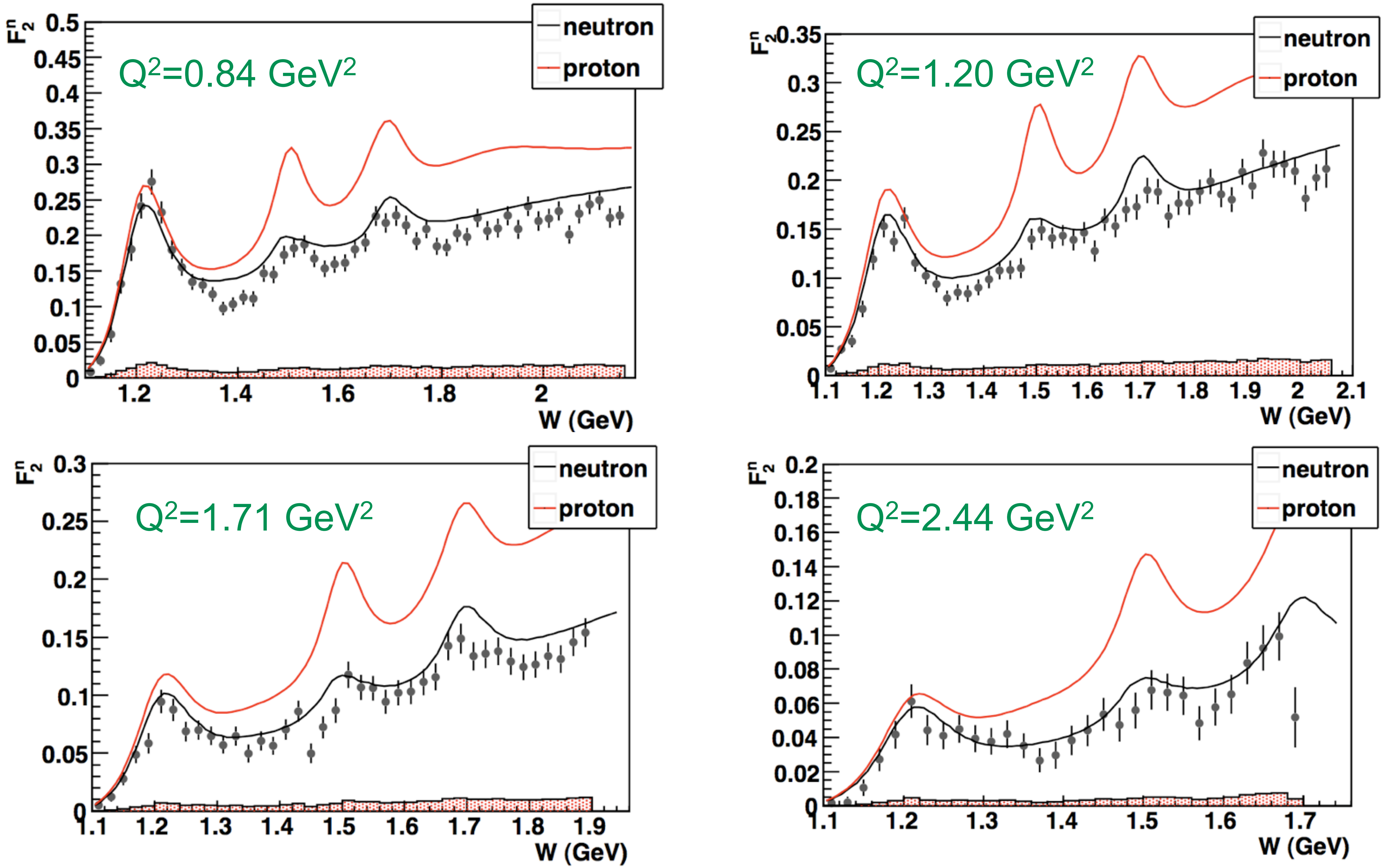

4 of 16 spectra: $0.8 < Q^2 < 4.5$; E_{beam} = 4.2 & 5.3 GeV; Bosted/Christy world fits

Final Data

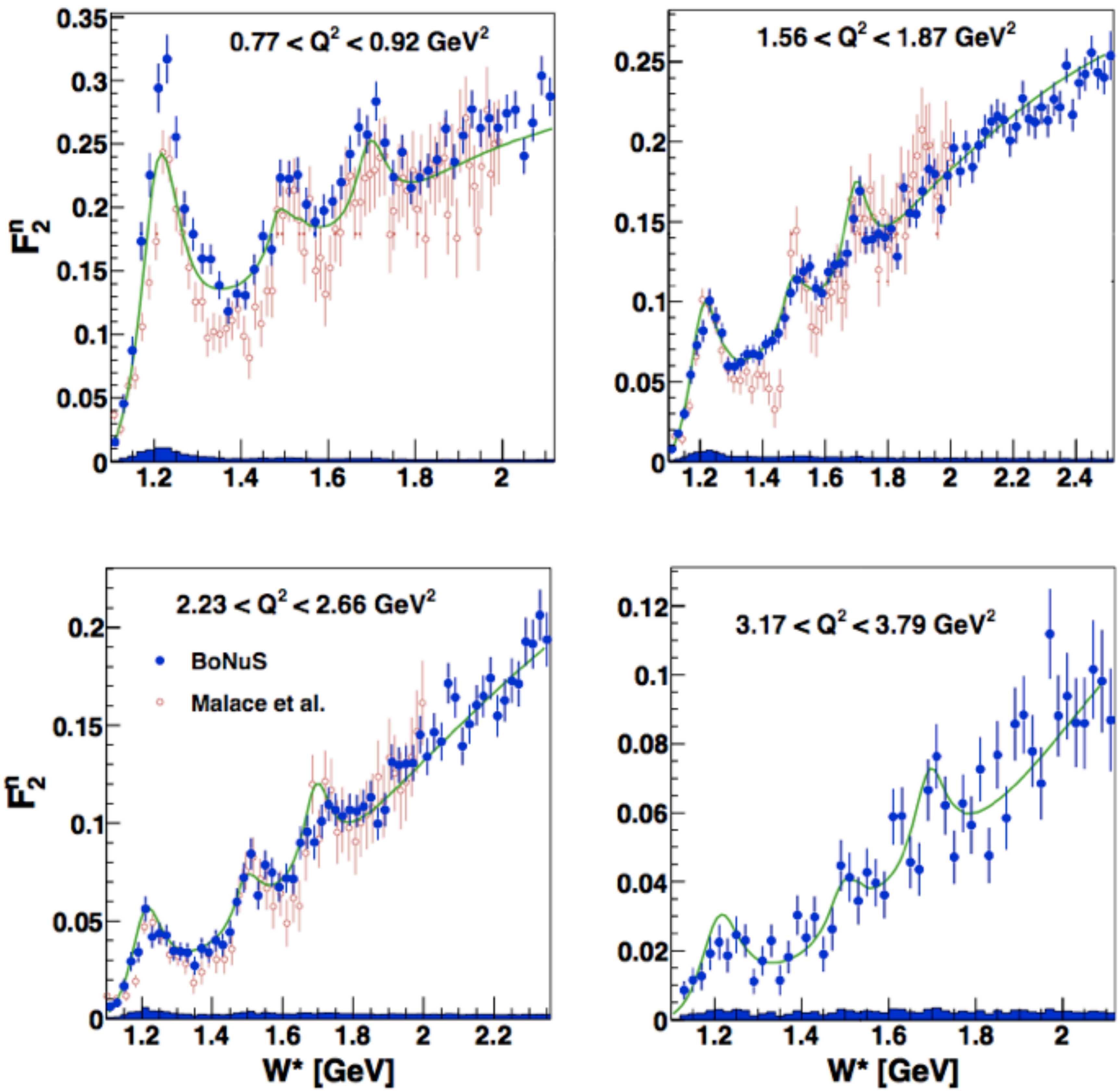

Various data compared to a state of the art nuclear physics extraction of neutron structure functions from deuterium (red points, Malace, et al.)

Deuteron EMC Effect

PHYSICAL REVIEW C **92**, 015211 (2015)

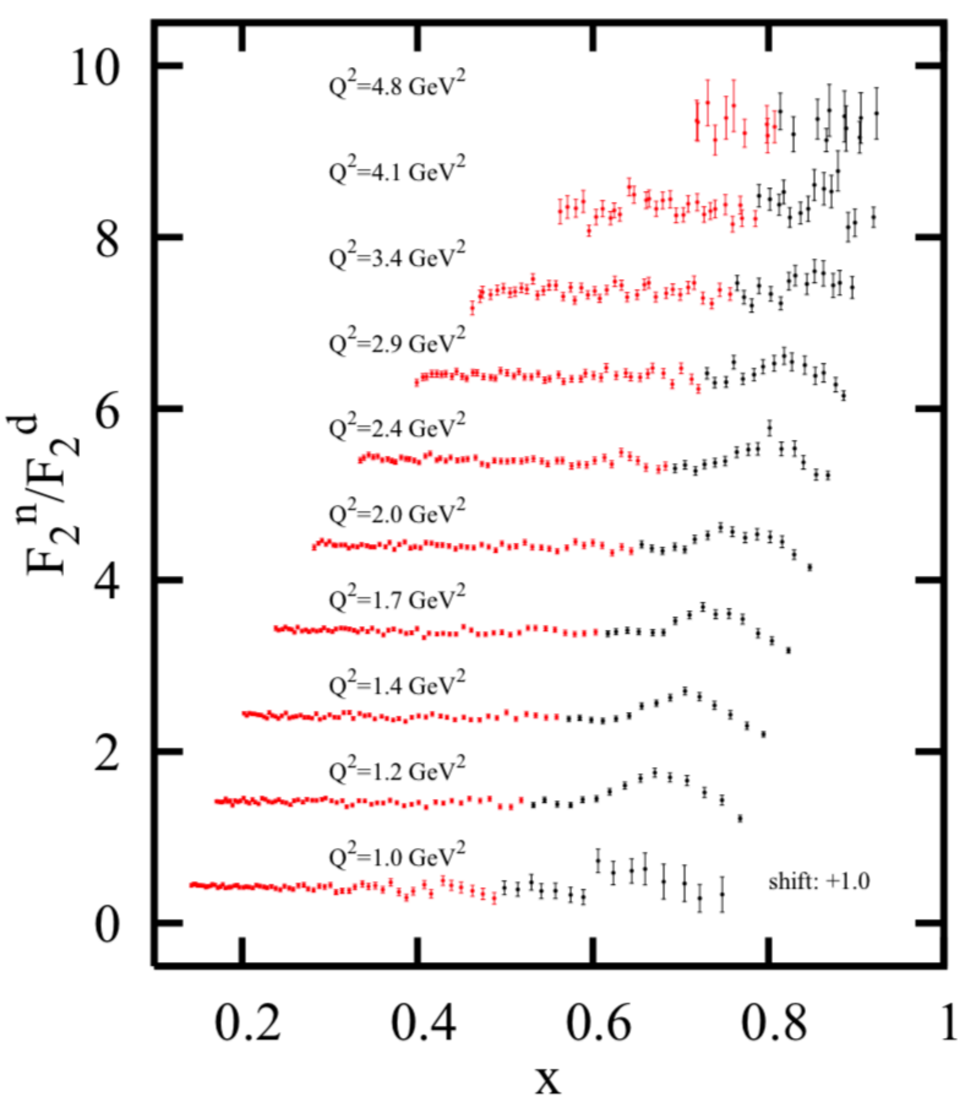

FIG. 1. (Color online) BONuS data for F_2^n/F_2^d vs Bjorken x taken with a 5.26-GeV beam. Only data for $Q^2 \geqslant 1$ GeV^2 are shown. The red points ($W > 1.4$ GeV) are used in this analysis. Error bars are statistical only. Each spectrum is shifted upward by 1.0 from the set below it.

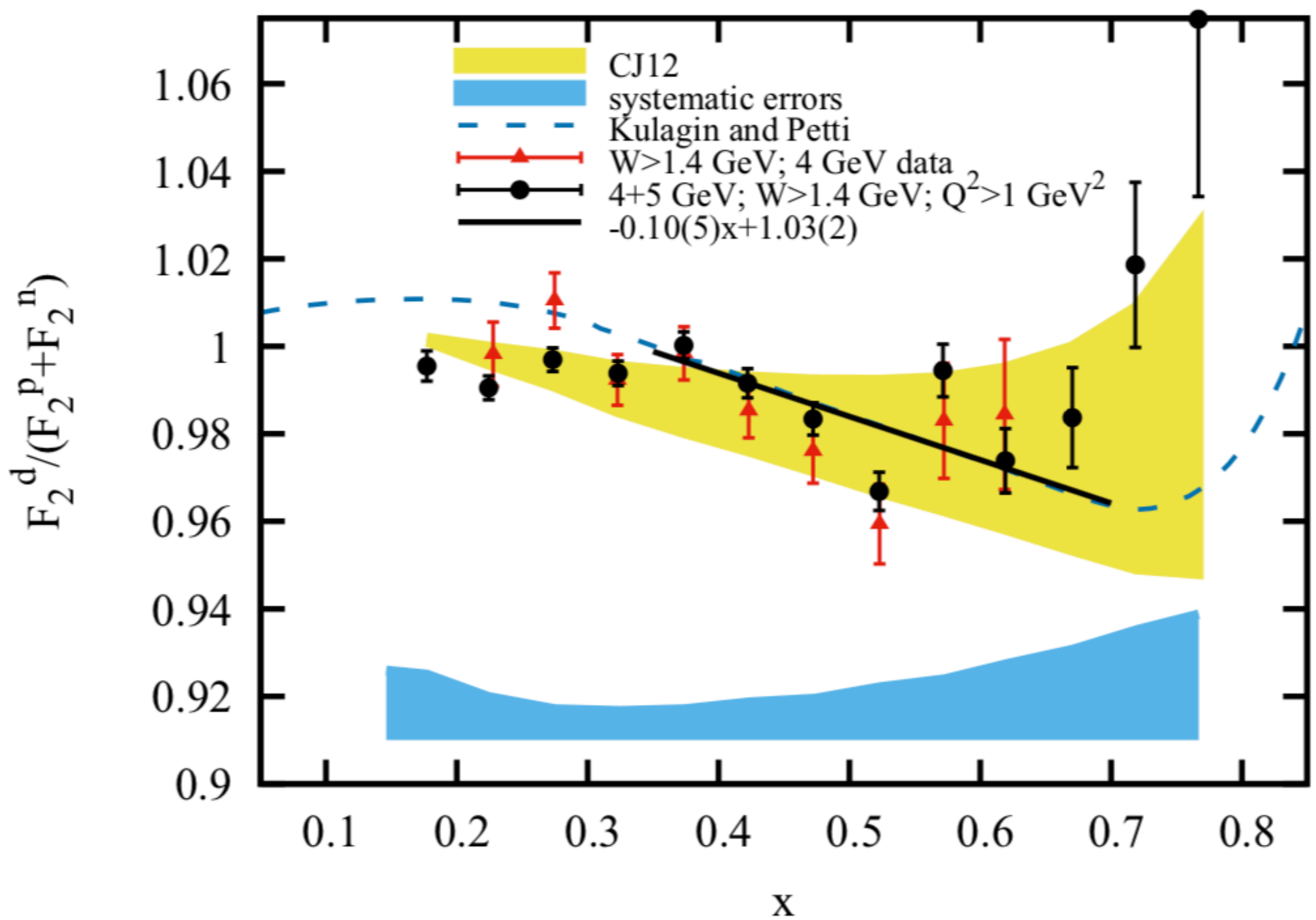

FIG. 2. (Color online) The deuteron EMC ratio $R^d_{\mathrm{EMC}} = F_2^d/(F_2^n + F_2^p)$ as extracted from the BONuS data. Total systematic uncertainties are shown as a band arbitrarily positioned at 0.91 (blue). The yellow band shows the CJ12 [49] limits expected from their nuclear models. The black points are the combined 4- and 5-GeV data, whereas the red points are the 4-GeV data alone. The dashed blue line shows the calculations of Ref. [36]. The solid line (black) is the fit to the black points for $0.35 < x < 0.7$.

Spin Structure Functions

Dynamic Nuclear Polarization:
- Freeze ammonia
- Make it paramagnetic through irradiation
- Put it into a 5 T magnetic field
- Drive transitions with microwaves
- Protons will accumulate into a single hyperfine state with spins aligned

Polarized Target

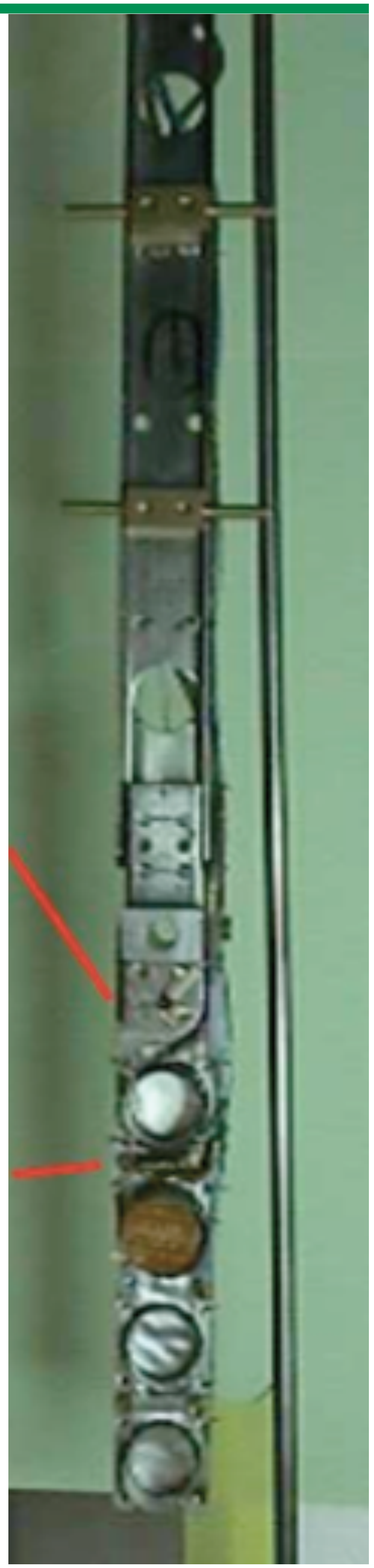

Asymmetries and g_1/F_1

Beam polarization

Target polarization

$$A_{\parallel} = \frac{1}{P_b P_t f} \frac{\sigma^{\downarrow\uparrow} - \sigma^{\uparrow\uparrow}}{\sigma^{\downarrow\uparrow} + \sigma^{\uparrow\uparrow}}$$

Dilution factor: ratio of scattering from protons to everything else in the target

Depolarization factor (photons are not in the beam direction)

tiny

small

small

$$\frac{A_{\parallel}}{D} = \frac{(1-\eta\gamma)g_1}{F_1} + \frac{\gamma(\eta-\gamma)g_2}{F_1}$$

WILLIAM & MARY
CHARTERED 1693

Polarized Structure Functions

PhysRevC.96.065208.pdf

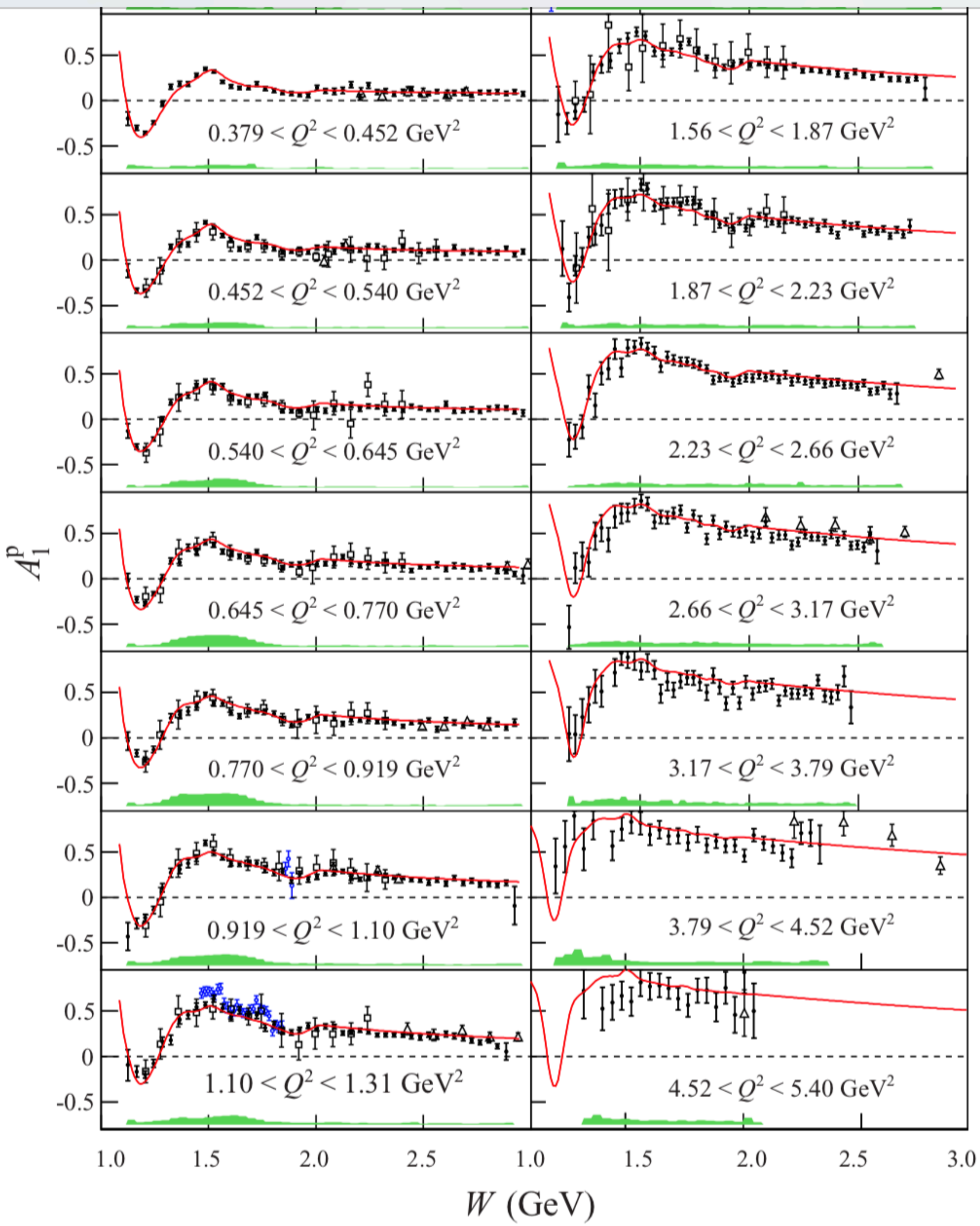

(x,Q^2)

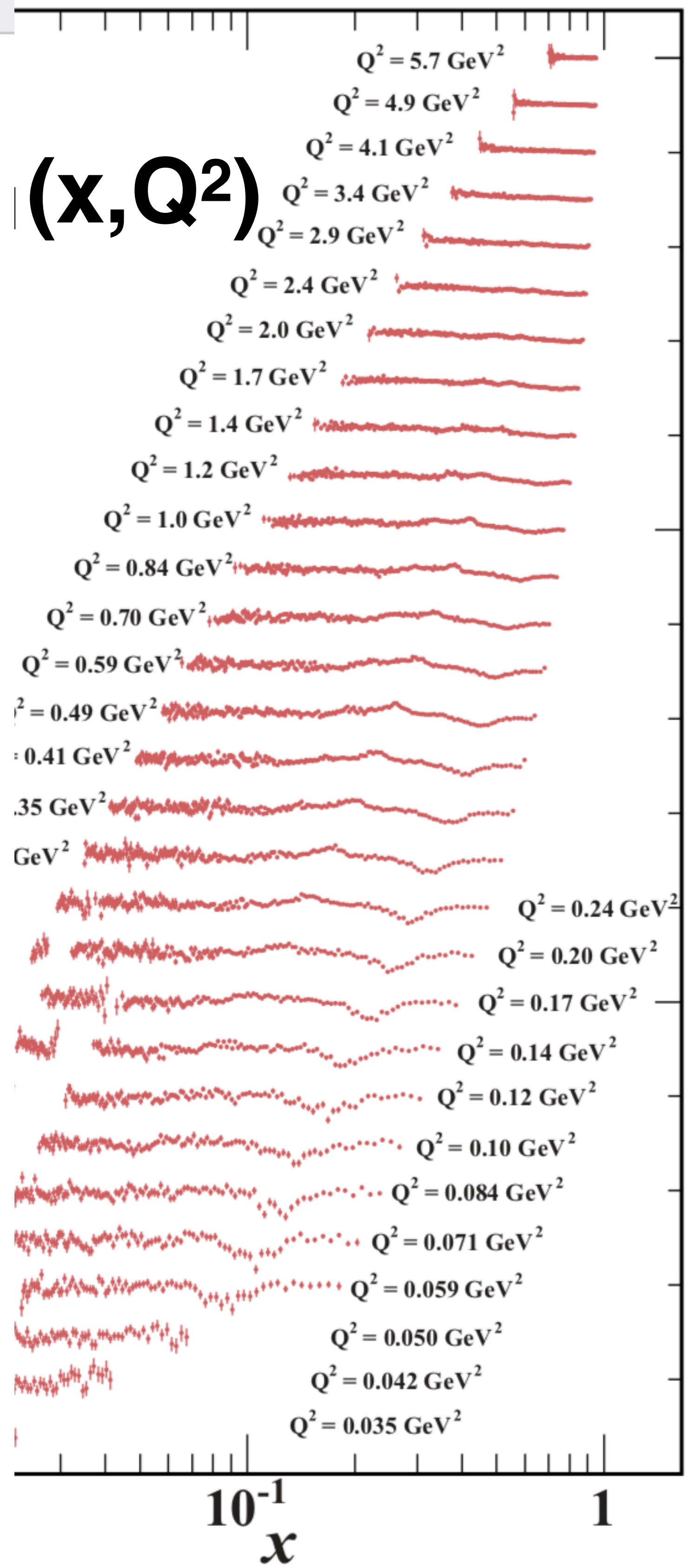

Moments

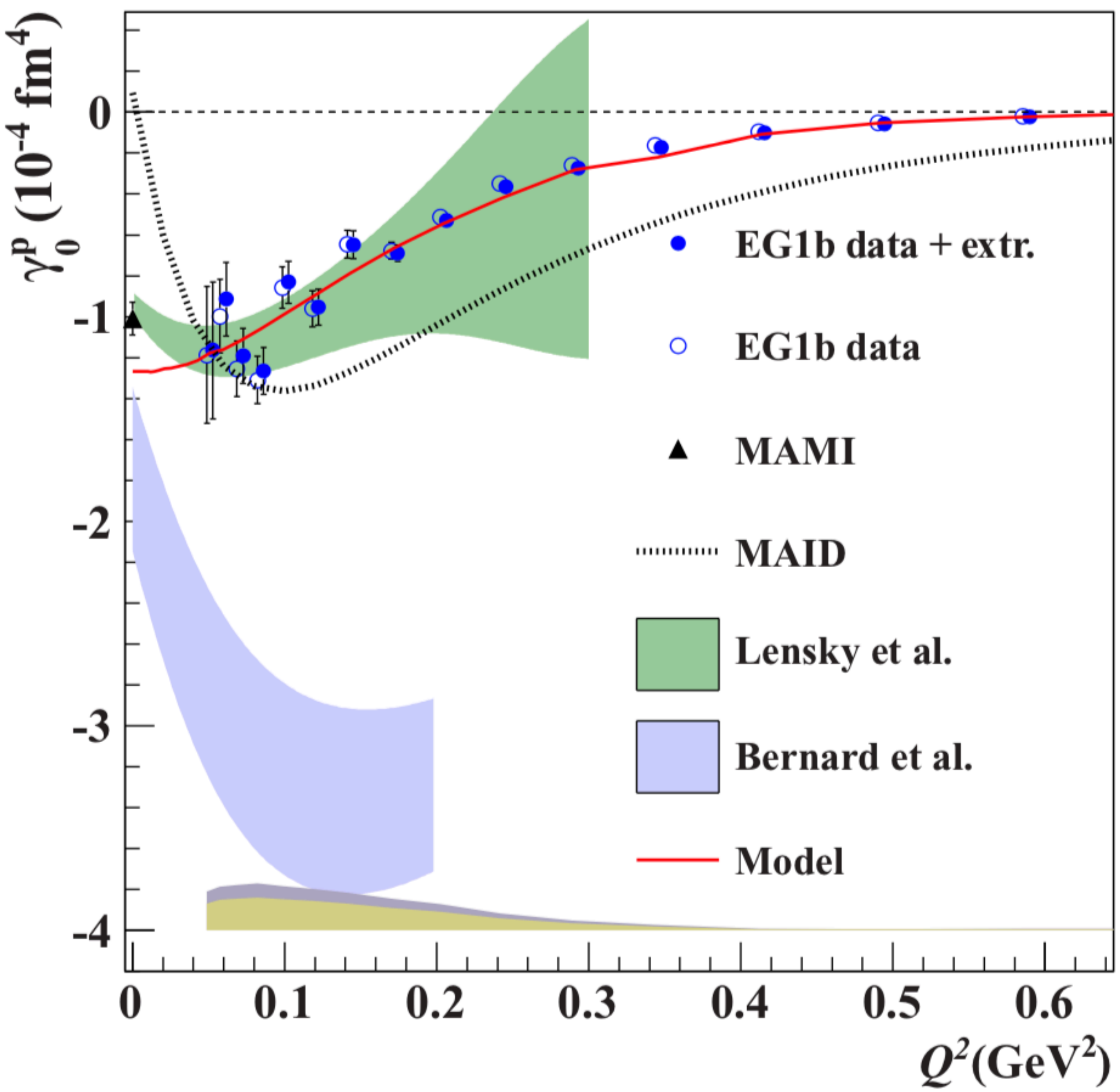

FIG. 38. The forward spin polarizability γ_0^p vs Q^2. Open and closed circles represent the contribution to the integral from the data only and the data plus model, respectively (slightly offset horizontally for clarity). Our model is shown as a solid red line. Our results are compared to χPT calculations (as in Fig. 35), the MAID parametrization for single-pion production, and real photon data at $Q^2 = 0$ from MAMI [141–143].

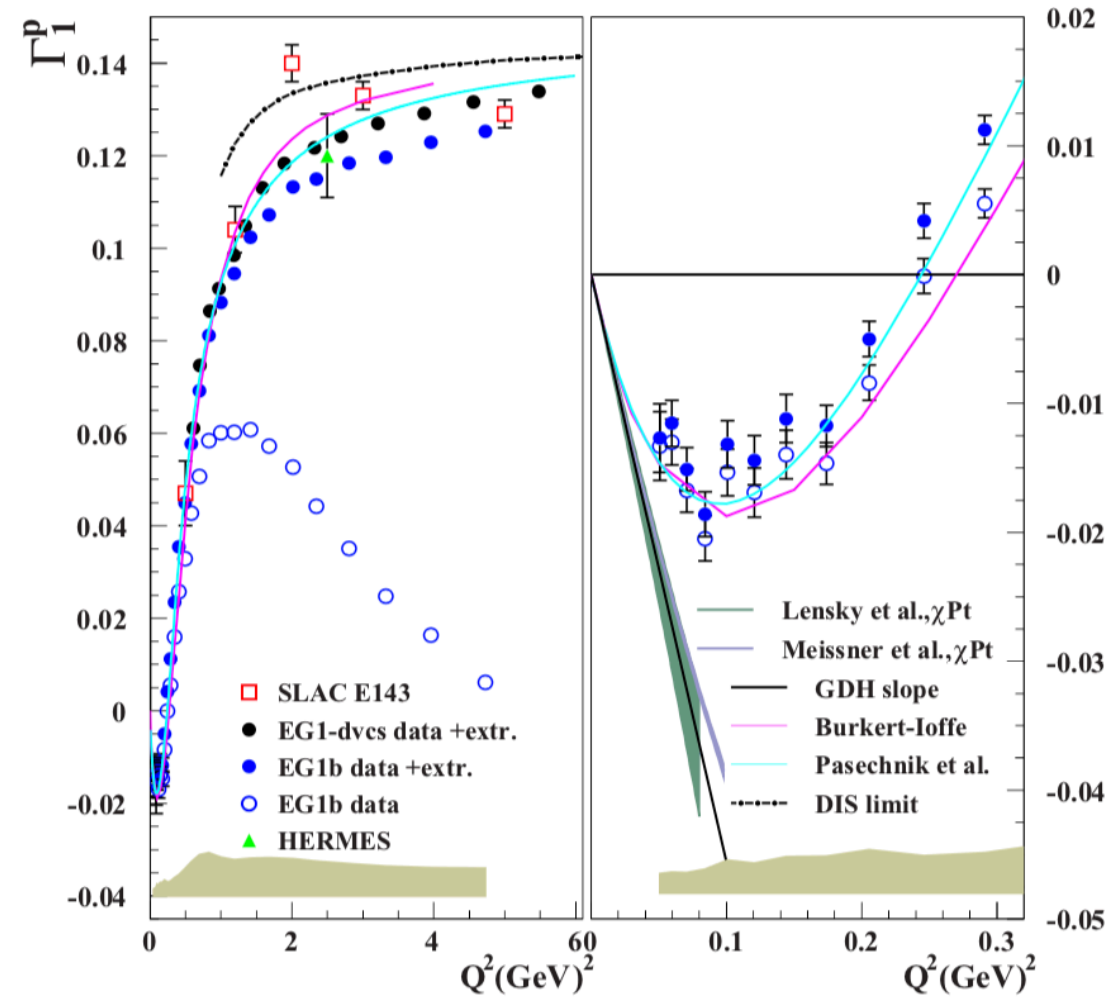

FIG. 35. Γ_1^p vs Q^2 for EG1b data and selected world data. The right panel shows an expanded scale at small Q^2. The open circles represent our data, integrated over the measured region. The filled blue circles are the full integral from $x = 0.001 \to 1$, excluding the elastic region. The curves show phenomenological parametrizations by Burkert and Ioffe [122,123] (magenta) and Pasechnik *et al.* [124] (cyan). The limiting cases of large Q^2 ("DIS limit") and $Q^2 \to 0$ ("GDH slope") are also shown, as well as two bands showing χPT calculations (Lensky *et al.* [125] and Meissner *et al.* [126]). The green band at the bottom represents the total systematic uncertainty.

Higher Twist Moments

Higher Twist Analysis of the Proton g_1 Structure Function

M. Osipenko[1], W. Melnitchouk[2], S. Simula[3], P. Bosted[2], V. Burkert[2],
M. E. Christy[4], K. Griffioen[5], C. Keppel[2,4], S. E. Kuhn[6]
[1] *INFN, Sezione di Genova, 16146, Genoa, Italy*
[2] *Jefferson Lab, 12000 Jefferson Avenue, Newport News, Virginia 23606, USA*
[3] *INFN, Sezione Roma III, 00146 Roma, Italy*
[4] *Hampton University, Hampton, Virginia 23668, USA*
[5] *College of William & Mary, Williamsburg, Virginia, 23187, USA*
[6] *Old Dominion University, Norfolk, Virginia 23529, USA*

We perform a global analysis of all available spin-dependent proton structure function data, covering a large range of Q^2, $1 \leq Q^2 \leq 30$ GeV^2, and calculate the lowest moment of the g_1 structure function as a function of Q^2. From the Q^2 dependence of the lowest moment we extract matrix elements of twist-4 operators, and determine the color electric and magnetic polarizabilities of the proton to be $\chi_E = 0.026 \pm 0.015$ (stat.) $\pm^{0.021}_{0.024}$ (sys.) and $\chi_B = -0.013 \mp 0.007$ (stat.) $\mp^{0.010}_{0.012}$ (sys.), respectively.

PACS numbers: 12.38.Aw, 12.38.Qk, 13.60.Hb

$$\chi_E = \frac{2}{3}(2d_2 + f_2)$$

$$\chi_B = \frac{1}{3}(4d_2 - f_2)$$

$$d_2(Q^2) = \int_0^1 dx\, x^2 \left[2g_1(x,Q^2) + 3g_2(x,Q^2)\right]$$

$$\chi_E = 0.026 \pm 0.015\ (\text{stat.}) \pm^{0.021}_{0.024}\ (\text{sys.})$$

$$\chi_B = -0.013 \mp 0.007\ (\text{stat.}) \mp^{0.010}_{0.012}\ (\text{sys.})$$

WILLIAM & MARY
CHARTERED 1693

PHYSICAL REVIEW A **83**, 042509 (2011)

Proton-structure corrections to hyperfine splitting in muonic hydrogen

Carl E. Carlson,[1,2] Vahagn Nazaryan,[3] and Keith Griffioen[2]
[1]*Helmholtz Institut Mainz, Johannes Gutenberg-Universität, D-55099 Mainz, Germany*
[2]*Department of Physics, College of William and Mary, Williamsburg, VA 23187, USA*
[3]*Center for Advanced Medical Instrumentation, Department of Physics, Hampton University, Hampton, VA 23668*
(Received 7 February 2011; published 19 April 2011)

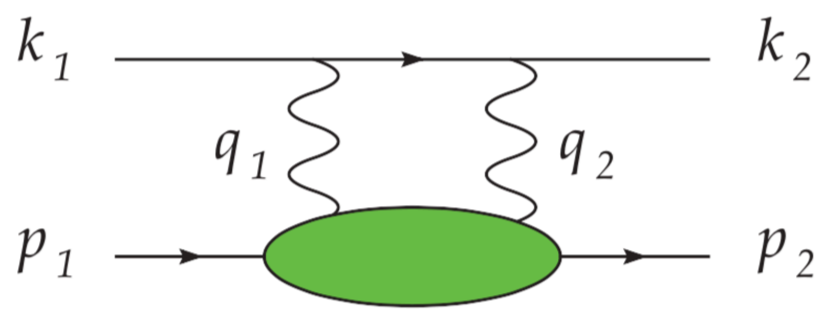

FIG. 1. (Color online) Diagram giving proton structure-dependent corrections to the hyperfine splitting.

$$\Delta_1 = \int_0^\infty \frac{dQ^2}{Q^2}\left\{\beta_1(\tau_\ell)F_2^2(Q^2) + 4m_p\int_{\nu_{th}}^\infty \frac{d\nu}{\nu^2}\,\frac{Q^4\beta_1(\tau)-4m_\ell^2\nu^2\beta_1(\tau_\ell)}{Q^4-4m_\ell^2\nu^2}\,g_1(\nu,Q^2)\right\},$$

$$\Delta_2 = -12m_p^2\int_0^\infty \frac{dQ^2}{Q^2}\int_{\nu_{th}}^\infty \frac{d\nu}{\nu^2}\,\frac{Q^4[\beta_2(\tau)-\beta_2(\tau_\ell)]}{Q^4-4m_\ell^2\nu^2}\,g_2(\nu,Q^2).$$

$$\Delta_S = \Delta_Z + \Delta_R + \Delta_{\rm pol} = \frac{E_{2\gamma}^{\rm box}}{E_F} - \frac{8\alpha m_r}{\pi}\int_0^\infty \frac{dQ}{Q^2}, \qquad (21)$$

called Zemach, recoil, and polarizability terms.

We have subtracted from the box diagram the iteration of the lowest order one-photon exchange diagram, since in a bound state calculation that contribution is already included [11]. This cancels the infrared divergence in the box diagram. The visible effect of the subtraction is to give the "-1" in the

$$\Delta_1 = \int_0^\infty \frac{dQ^2}{Q^2}\left\{\beta_1(\tau_\ell)F_2^2(Q^2) + 4m_p\int_{\nu_{th}}^\infty \frac{d\nu}{\nu^2}\,\frac{Q^4\beta_1(\tau)-4m_\ell^2\nu^2\beta_1(\tau_\ell)}{Q^4-4m_\ell^2\nu^2}\,g_1(\nu,Q^2)\right\},$$

$$\Delta_2 = -12m_p^2\int_0^\infty \frac{dQ^2}{Q^2}\int_{\nu_{th}}^\infty \frac{d\nu}{\nu^2}\,\frac{Q^4[\beta_2(\tau)-\beta_2(\tau_\ell)]}{Q^4-4m_\ell^2\nu^2}\,g_2(\nu,Q^2)$$

The Zemach term is

$$\Delta_Z = \frac{8\alpha m_r}{\pi}\int_0^\infty \frac{dQ}{Q^2}\left(\frac{G_E(Q^2)G_M(Q^2)}{1+\kappa_p} - 1\right) \equiv -2\alpha m_r r_Z, \qquad (22)$$

where r_Z is the Zemach radius. The first part of the Zemach term is obtained from the first line of Eq. (20) with $\beta_1(\tau_i)$ replaced by the first term in its low argument limit and F_1 replaced by G_E. The Zemach term is finite in the nonrelativistic

$$E_{\rm HFS}^{2S} = 22.8146(49)\ \text{meV}$$

TMDs

- Any confined quark must have transverse momentum
- Therefore, colinear PDFs cannot give the whole story
- Transverse momentum is related to L_z
- There has been much recent work trying to understand transverse momentum distributions (TMDs)

$x f_1^u(x)$

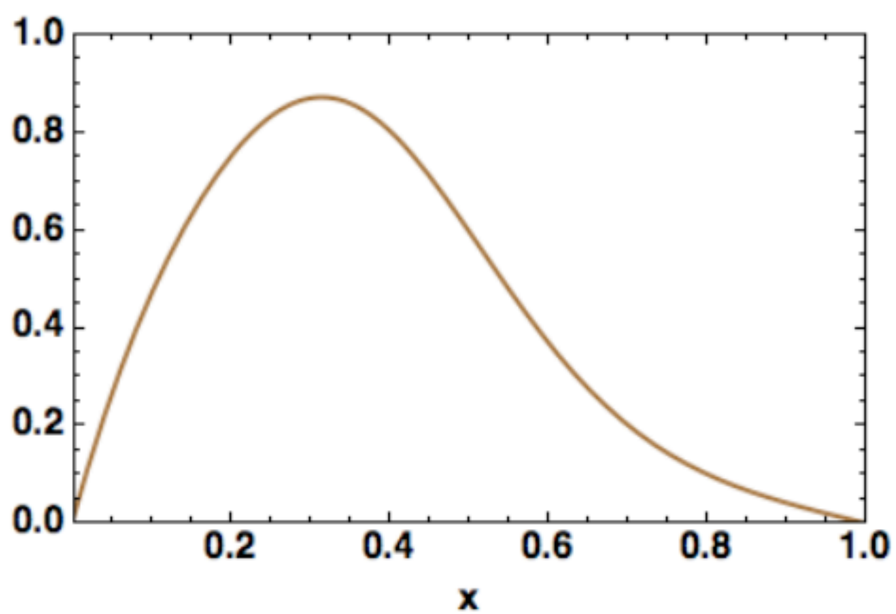

Standard collinear PDF

$x f_1^u(x, p_T^2)$

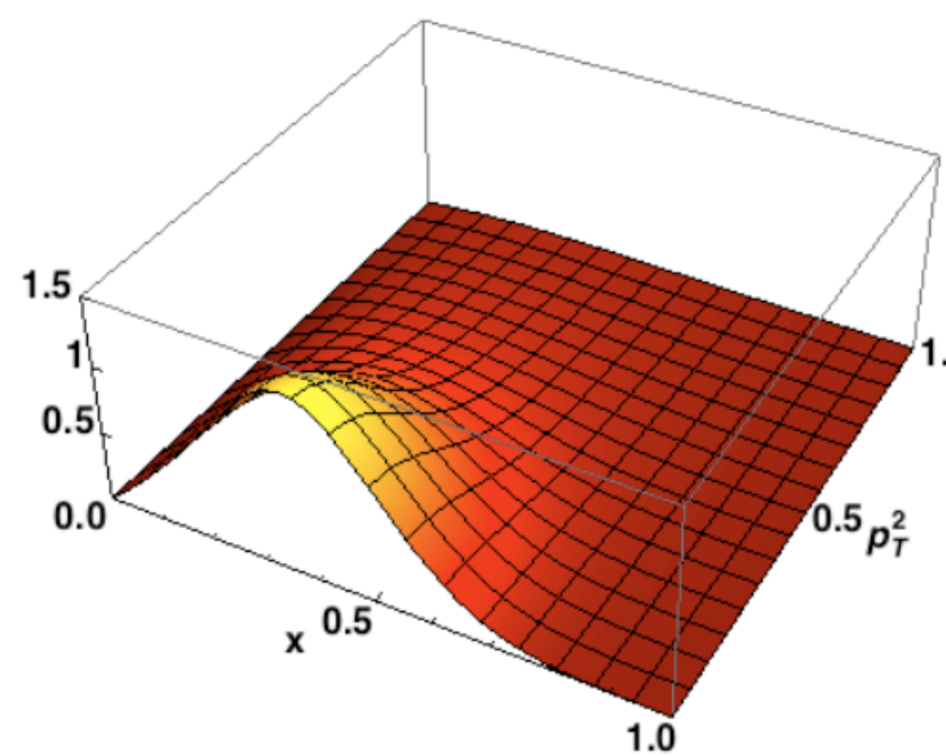

TMD

Semi-Inclusive DIS

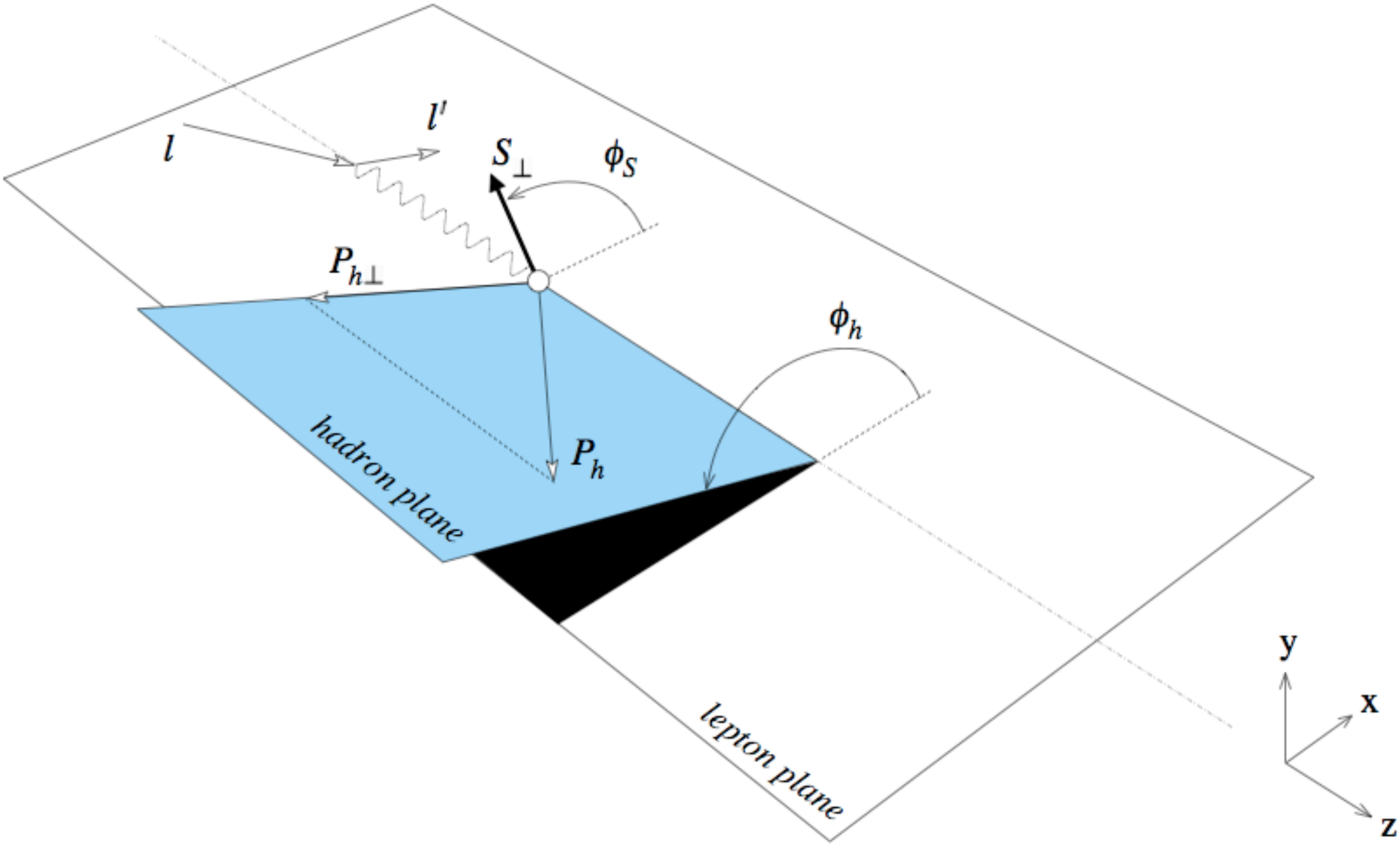

SIDIS Cross Section

$$\frac{d\sigma}{dx\,dy\,d\psi\,dz\,d\phi_h\,dP_{h\perp}^2} =$$

Bacchetta, et al., JHEP 2(2007)093

$$\frac{\alpha^2}{xyQ^2}\frac{y^2}{2(1-\varepsilon)}\left(1+\frac{\gamma^2}{2x}\right)\Big\{F_{UU,T}+\varepsilon F_{UU,L}+\sqrt{2\varepsilon(1+\varepsilon)}\cos\phi_h\,F_{UU}^{\cos\phi_h}$$

$$+\varepsilon\cos(2\phi_h)\,F_{UU}^{\cos 2\phi_h}+\lambda_e\sqrt{2\varepsilon(1-\varepsilon)}\sin\phi_h\,F_{LU}^{\sin\phi_h}$$

$$+S_\parallel\left[\sqrt{2\varepsilon(1+\varepsilon)}\sin\phi_h\,F_{UL}^{\sin\phi_h}+\varepsilon\sin(2\phi_h)\,F_{UL}^{\sin 2\phi_h}\right]$$

$$+S_\parallel\lambda_e\left[\sqrt{1-\varepsilon^2}\,F_{LL}+\sqrt{2\varepsilon(1-\varepsilon)}\cos\phi_h\,F_{LL}^{\cos\phi_h}\right]$$

$$+|\boldsymbol{S}_\perp|\Big[\sin(\phi_h-\phi_S)\left(F_{UT,T}^{\sin(\phi_h-\phi_S)}+\varepsilon F_{UT,L}^{\sin(\phi_h-\phi_S)}\right)$$

$$+\varepsilon\sin(\phi_h+\phi_S)\,F_{UT}^{\sin(\phi_h+\phi_S)}+\varepsilon\sin(3\phi_h-\phi_S)\,F_{UT}^{\sin(3\phi_h-\phi_S)}$$

$$+\sqrt{2\varepsilon(1+\varepsilon)}\sin\phi_S\,F_{UT}^{\sin\phi_S}+\sqrt{2\varepsilon(1+\varepsilon)}\sin(2\phi_h-\phi_S)\,F_{UT}^{\sin(2\phi_h-\phi_S)}\Big]$$

$$+|\boldsymbol{S}_\perp|\lambda_e\Big[\sqrt{1-\varepsilon^2}\cos(\phi_h-\phi_S)\,F_{LT}^{\cos(\phi_h-\phi_S)}+\sqrt{2\varepsilon(1-\varepsilon)}\cos\phi_S\,F_{LT}^{\cos\phi_S}$$

$$+\sqrt{2\varepsilon(1-\varepsilon)}\cos(2\phi_h-\phi_S)\,F_{LT}^{\cos(2\phi_h-\phi_S)}\Big]\Big\},$$

Leading Twist

Sub-Leading Twist (extra factor of 1/Q)

0 (i.e. $R=\sigma_L/\sigma_T=0$)

A_{UL} = {UL terms} / {UU terms}

A_{LL} = {LL terms} / {UU terms}

etc.

TMDs in Eg1-dvcs

$$F_{UU,T} = \mathcal{C}\left[f_1 D_1\right] \qquad F_{UU,L} = 0 \qquad F_{UU}^{\cos 2\phi_h} = \mathcal{C}\left[-\frac{2\left(\hat{\boldsymbol{h}}\cdot\boldsymbol{k}_T\right)\left(\hat{\boldsymbol{h}}\cdot\boldsymbol{p}_T\right) - \boldsymbol{k}_T\cdot\boldsymbol{p}_T}{M M_h} h_1^{\perp} H_1^{\perp}\right]$$

$$F_{UU}^{\cos\phi_h} = \frac{2M}{Q}\mathcal{C}\left[-\frac{\hat{\boldsymbol{h}}\cdot\boldsymbol{k}_T}{M_h}\left(xh\, H_1^{\perp} + \frac{M_h}{M} f_1 \frac{\tilde{D}^{\perp}}{z}\right) - \frac{\hat{\boldsymbol{h}}\cdot\boldsymbol{p}_T}{M}\left(xf^{\perp} D_1 + \frac{M_h}{M} h_1^{\perp} \frac{\tilde{H}}{z}\right)\right]$$

$$F_{LU}^{\sin\phi_h} = \frac{2M}{Q}\mathcal{C}\left[-\frac{\hat{\boldsymbol{h}}\cdot\boldsymbol{k}_T}{M_h}\left(xe\, H_1^{\perp} + \frac{M_h}{M} f_1 \frac{\tilde{G}^{\perp}}{z}\right) + \frac{\hat{\boldsymbol{h}}\cdot\boldsymbol{p}_T}{M}\left(xg^{\perp} D_1 + \frac{M_h}{M} h_1^{\perp} \frac{\tilde{E}}{z}\right)\right]$$

$$F_{UL}^{\sin 2\phi_h} = \mathcal{C}\left[-\frac{2\left(\hat{\boldsymbol{h}}\cdot\boldsymbol{k}_T\right)\left(\hat{\boldsymbol{h}}\cdot\boldsymbol{p}_T\right) - \boldsymbol{k}_T\cdot\boldsymbol{p}_T}{M M_h} h_{1L}^{\perp} H_1^{\perp}\right]$$

$$F_{UL}^{\sin\phi_h} = \frac{2M}{Q}\mathcal{C}\left[-\frac{\hat{\boldsymbol{h}}\cdot\boldsymbol{k}_T}{M_h}\left(xh_L H_1^{\perp} + \frac{M_h}{M} g_{1L} \frac{\tilde{G}^{\perp}}{z}\right) + \frac{\hat{\boldsymbol{h}}\cdot\boldsymbol{p}_T}{M}\left(xf_L^{\perp} D_1 - \frac{M_h}{M} h_{1L}^{\perp} \frac{\tilde{H}}{z}\right)\right]$$

$$F_{LL} = \mathcal{C}\left[g_{1L} D_1\right]$$

$$F_{LL}^{\cos\phi_h} = \frac{2M}{Q}\mathcal{C}\left[\frac{\hat{\boldsymbol{h}}\cdot\boldsymbol{k}_T}{M_h}\left(xe_L H_1^{\perp} - \frac{M_h}{M} g_{1L} \frac{\tilde{D}^{\perp}}{z}\right) - \frac{\hat{\boldsymbol{h}}\cdot\boldsymbol{p}_T}{M}\left(xg_L^{\perp} D_1 + \frac{M_h}{M} h_{1L}^{\perp} \frac{\tilde{E}}{z}\right)\right]$$

CLAS Collaboration (S. Jawalkar (William-Mary Coll.) *et al.*). Sep 21, 2017. 6 pp.
Published in **Phys.Lett. B782 (2018) 662-667**

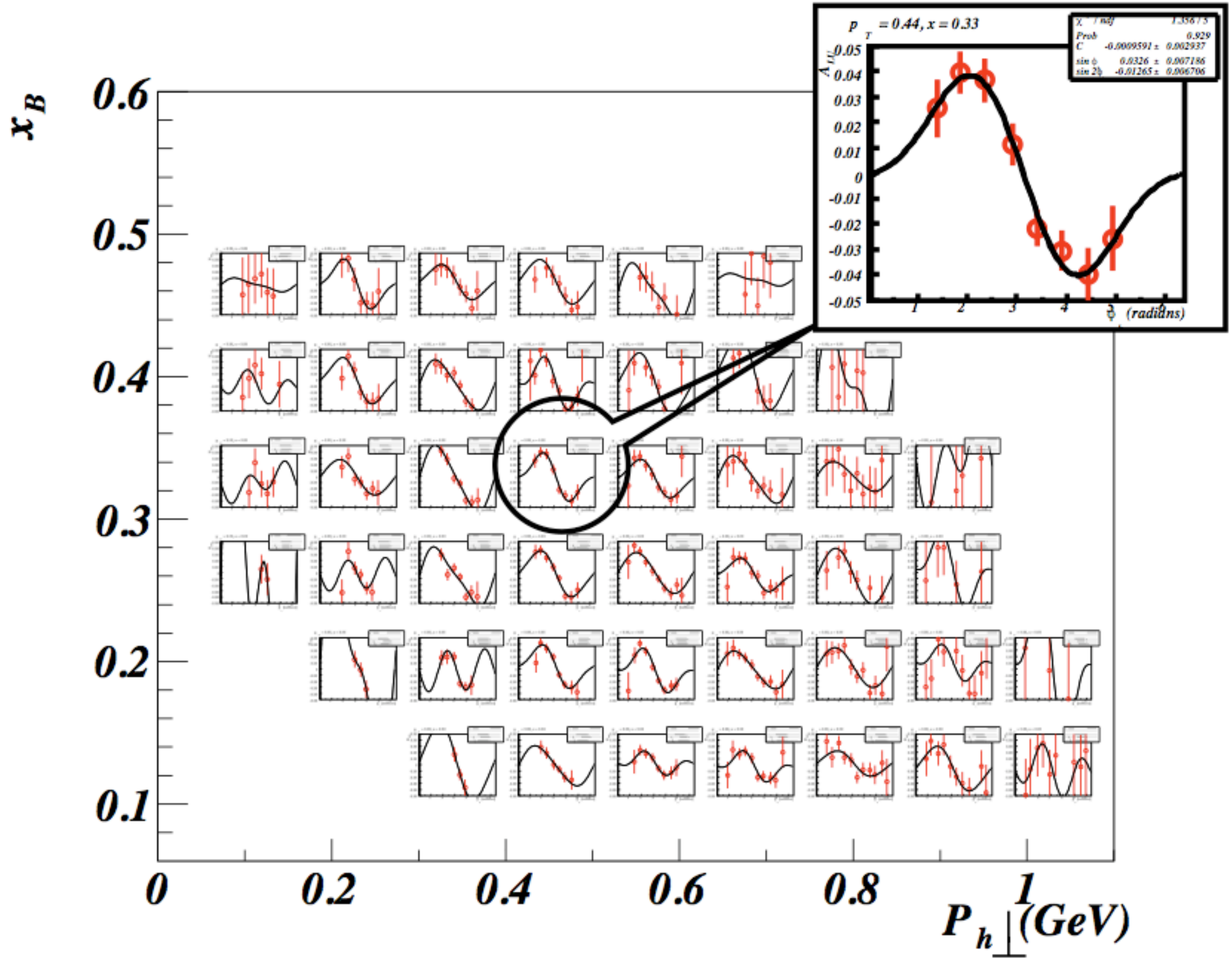

Dihadron SIDIS

Bacchetta, PR**D69**(2004)074026

$$d^7\sigma_{OO}=\frac{\alpha^2}{2\pi Q^2 y}\sum_a e_a^2\left\{A(y)f_1(x)D_1(z,\zeta,M_h^2)-V(y)\cos\phi_R\frac{|\vec{R}_T|}{Q}\left[\frac{1}{z}f_1(x)\tilde{D}^{\sphericalangle}(z,\zeta,M_h^2)+\frac{M}{M_h}xh(x)H_1^{\sphericalangle}(z,\zeta,M_h^2)\right]\right\}$$

$$d^7\sigma_{LO}=\frac{\alpha^2}{2\pi Q^2 y}\lambda\sum_a e_a^2 W(y)\sin\phi_R\frac{|\vec{R}_T|}{Q}\left[\frac{M}{M_h}xe(x)H_1^{\sphericalangle}(z,\zeta,M_h^2)+\frac{1}{z}f_1(x)\tilde{G}^{\sphericalangle}(z,\zeta,M_h^2)\right]$$

$$d^7\sigma_{OL}=\frac{\alpha^2}{2\pi Q^2 y}S_L\sum_a e_a^2 V(y)\sin\phi_R\frac{|\vec{R}_T|}{Q}\left[\frac{M}{M_h}xh_L(x)H_1^{\sphericalangle}(z,\zeta,M_h^2)+\frac{1}{z}g_1(x)\tilde{G}^{\sphericalangle}(z,\zeta,M_h^2)\right]$$

$$d^7\sigma_{OT}=\frac{\alpha^2}{2\pi Q^2 y}|\vec{S}_\perp|\sum_a e_a^2\left\{B(y)\sin(\phi_R+\phi_S)\frac{|\vec{R}_T|}{M_h}h_1(x)H_1^{\sphericalangle}(z,\zeta,M_h^2)\right.$$

$$\left.+V(y)\sin\phi_S\frac{M_h}{Q}\left[h_1(x)\left(\frac{1}{z}\tilde{H}(z,\zeta,M_h^2)+\frac{|\vec{R}_T|^2}{M_h^2}H_1^{\sphericalangle\ o(1)}(z,\zeta,M_h^2)\right)-\frac{M}{M_h}xf_T(x)D_1(z,\zeta,M_h^2)\right]\right\}$$

$$d^7\sigma_{LT}=\frac{\alpha^2}{2\pi Q^2 y}\lambda|\vec{S}_\perp|\sum_a e_a^2 W(y)\cos\phi_S\frac{M_h}{Q}\left[-\frac{M}{M_h}xg_T(x)D_1(z,\zeta,M_h^2)-\frac{1}{z}h_1(x)\tilde{E}(z,\zeta,M_h^2)\right]$$

$$d^7\sigma_{LL}=\frac{\alpha^2}{2\pi Q^2 y}\lambda S_L\sum_a e_a^2\left\{C(y)g_1(x)D_1(z,\zeta,M_h^2)-W(y)\cos\phi_R\frac{|\vec{R}_T|}{Q}\left[\frac{1}{z}g_1(x)\tilde{D}^{\sphericalangle}(z,\zeta,M_h^2)\right.\right.$$

$$\left.\left.-\frac{M}{M_h}xe_L(x)H_1^{\sphericalangle}(z,\zeta,M_h^2)\right]\right\},$$

$$\zeta=\frac{1}{M_h}\left(\sqrt{M_1^2-|\vec{R}|^2}-\sqrt{M_2^2-|\vec{R}|^2-2|\vec{R}|\cos\theta}\right)$$

Leading Twist

Sub-Leading Twist (extra factor of 1/Q)

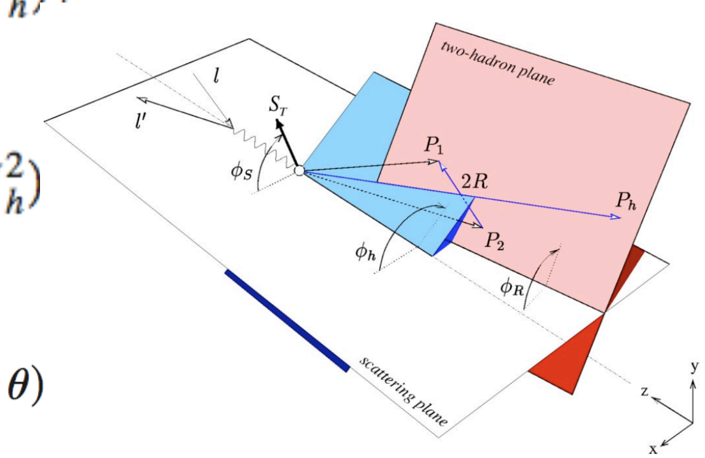

Proton Radius

Pohl, doi:10.1146/annurev-nucl-102212-170627

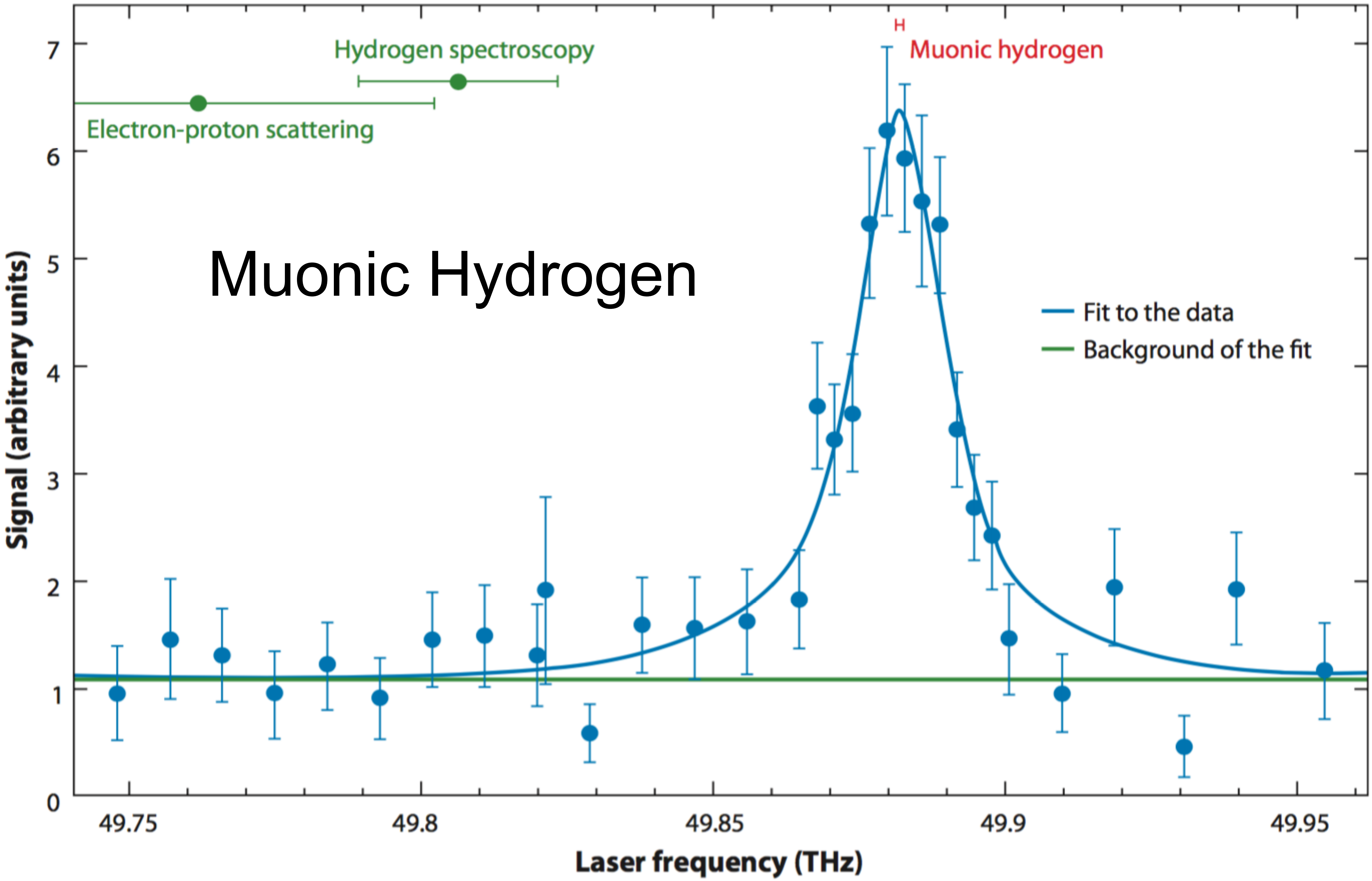

PRAD in Hall B

$$, r_p = 0.831 \pm 0.007_{stat} \pm 0.012_{syst} \text{ femtometres},$$

Article | Published: 06 November 2019

A small proton charge radius from an electron–proton scattering experiment

W. Xiong, A. Gasparian, [...] Z. W. Zhao

Nature **575**, 147–150(2019) | Cite this article

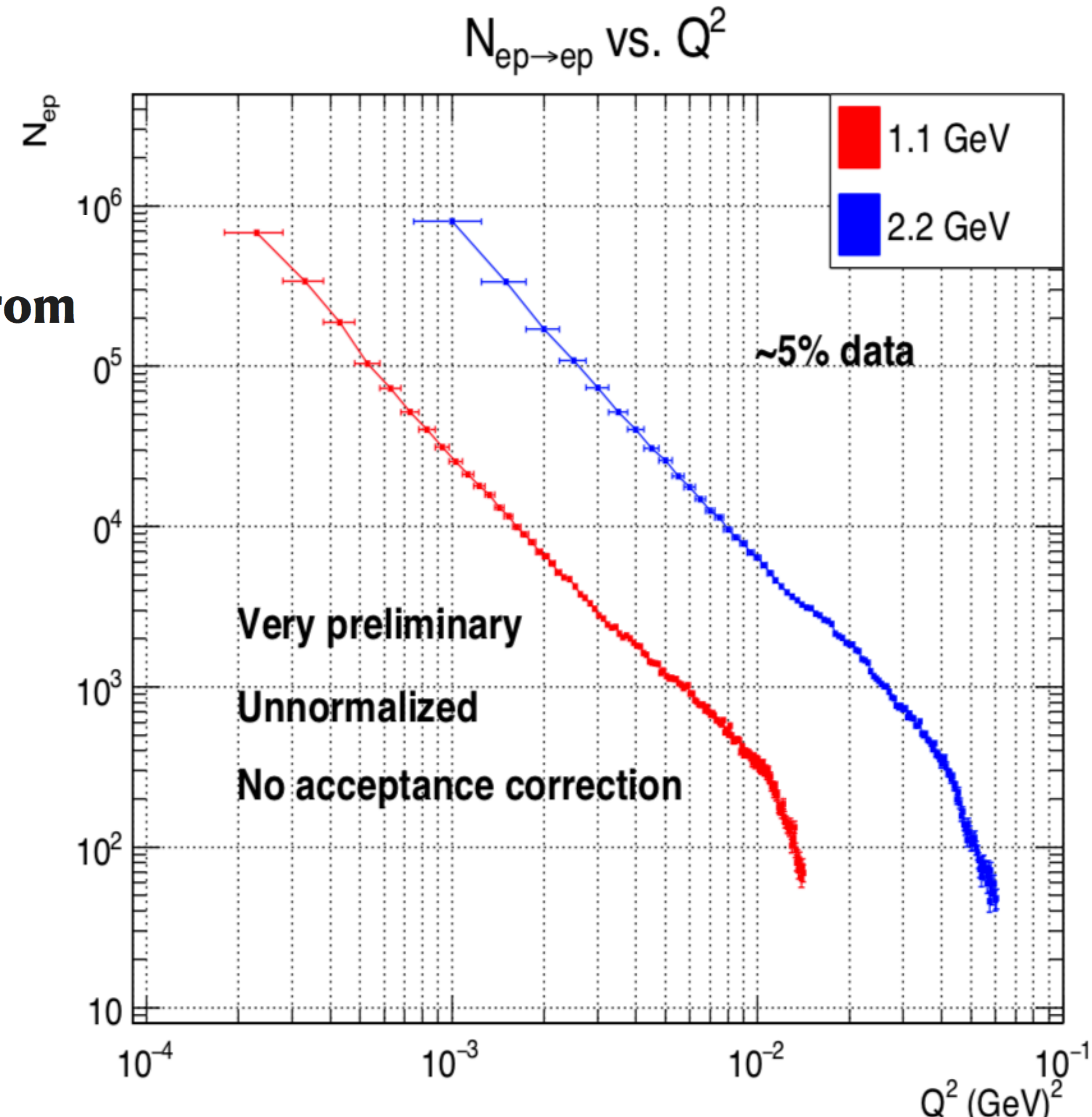

The NIST Reference on
Constants, Units, and Uncertainty

Constants Topics:

Values

Energy Equivalents

Searchable Bibliography

Background

Constants Bibliography

Constants, Units & Uncertainty home page

Fundamental Physical Constants

proton rms charge radius

r_{p}

Numerical value	8.414×10^{-16} m
Standard uncertainty	0.019×10^{-16} m
Relative standard uncertainty	2.2×10^{-3}
Concise form	$8.414(19) \times 10^{-16}$ m

Click here for **correlation coefficient** of this constant with other constants

Source: 2018 CODATA recommended values

Definition of uncertainty

Correlation coefficient with any other constant

Volker has encouraged, funded, and
enabled all of us to
lay the groundwork for a full
understanding of the nucleon
with 12 GeV and eventually
with EIC Femtography

Thank you!

Fine